AFCRC Technical Report 53-7

GEOPHYSICAL RESEARCH PAPERS

No. 20

ON THE PHENOMENON OF THE COLORED SUN, ESPECIALLY THE "BLUE" SUN OF SEPTEMBER 1950

RUDOLF PENNDORF

April 1953

Geophysics Research Directorate

Air Force Cambridge Research Center

Cambridge Massachusetts

ABSTRACT

The phenomenon of a colored sun or moon can be explained by Mie's theory of large particle scattering, if the radius of such particles is of the order of the wavelength of light.

Smoke generated by large forest fires in Alberta, Canada, traveled across the Atlantic. In many places in the eastern United States and especially over large parts of Europe, the sun, moon and stars were seen blue in color in September 1950. Using Mie's theory and some extinction measurements, the radius of the particles is calculated to be between 0.5 and 0.8 μ and the concentration 175/cm^3 and 127/cm^3. The total amount in the smoke layer is about 4.7 to 6.5 $\times$ 10^7/cm^2 column. Three size spectra are assumed, case 1 deals with a uniform size, cases 2 and 3 with a Gaussian distribution of the size spectrum. The refractive index for water droplets is chosen, but it is also studied carefully for other substances. The radius becomes larger for ice at low temperatures and smaller for pure smoke; the total number varies inversely to the radius, but the extinction coefficient remains unchanged. Scattering by spherical particles is assumed, because the shape plays a very minor role. For anisotropic particles, the extinction coefficient increases by less than 10 percent.

The intensity distribution of the solar spectrum is calculated between 3500 Å and 7000 Å after passing through the smoke layer. The computations show that a pronounced maximum of the solar spectrum occurs around 4100 Å and 4600 Å in all the cases considered. The physiological impression of such a spectrum is bluish. It could be shown that the "blue" sun observed during dust storms can be explained in the same way if the radius of the quartz particles is about 0.3 μ and a total number $> 10^8$/cm^2. Finally the hypothetical case for a "green" sun is calculated. The computations show that this phenomenon can occur only for a narrow Gaussian distribution of particles and this explains the rareness of the phenomenon.

CONTENTS

ILLUSTRATIONS

ON THE PHENOMENON OF THE COLORED SUN, ESPECIALLY THE "BLUE" SUN OF SEPTEMBER 1950 *

1. COLORED SUN AND LARGE PARTICLE SCATTERING

The phenomenon of a colored sun or moon is not so unusual as it seems at first. Numerous descriptions of it exist in meteorological literature and a historical review is given by Rodewald (1952). It occurs only under certain favorable conditions in connection with (a) dust storms near loess† areas or deserts, (b) volcanic ash clouds after volcanic eruptions and (c) large forest fires or prairie fires. It can easily be observed under artificial conditions when homogeneous water droplets or aerosols are produced in large quantity. The "blue" sun and moon of September 1950 was observed over so large an area for several days that many reports have been published.

Before dealing with the phenomenon of September 1950, it seems necessary to state in general terms under what conditions a blue or green sun or moon can be observed. It is certainly due to scattering by large particles, where large means that the radius r of the particles is comparable to the wavelength λ of light. As long as $r \leqq 1/10\ \lambda$, Rayleigh scattering applies, which states that the extinction is proportional to λ^{-4} leading always to large values of extinction in the blue and small ones in the red. In order to get a blue or green sun, the extinction must be small in the blue or green, just inverse to the extinction due to Rayleigh scattering. This occurs only if $r > 1/10\,\lambda$, especially if $r \approx \lambda$ and can be explained by Mie's theory.

Let the cross section of extinction be E times the geometric cross section of the particles; E is called the efficiency factor. Then the extinction coefficient

$$\gamma = \pi r^2 N E(\alpha, m), \tag{1}$$

where all particles are supposed to have the same radius r, and N is their number per unit volume. The formulas of Mie give E as a function of the refractive index m and the size parameter α defined by

$$\alpha = 2\pi r/\lambda = 2\pi r n \tag{2}$$

with $n =$ the wave number.

A simplified diagram of the function $E(\alpha)$ is reproduced in Fig. 1, showing various maxima. Whenever the extinction curve is rising, as in parts a, c and e, light of longer wavelength will be scattered less than that of shorter wavelength, as in Rayleigh scattering. But whenever the extinction is decreasing with increasing α, as in parts b and d, the opposite will be true. In order to get a blue sun, the extinction must be larger in the red than in the blue and that means the particle size must be such that part b is the effective region for the wavelength of visible light. If, however, the sun appears green, the extinction must possess a minimum in the green and be large toward the red as well as toward the blue. In this case the radius must be such that the minimum between b and c is effective.

It will be shown later in Section 4.12 that a size spectrum will diminish considerably the amplitude of the oscillations after the first peak. Thus, the extinction by very large particles responsible for parts c,

* Manuscript received for publication 7 August 1952.

† Loess is a fine-grained, wind-blown deposit of alluvial age. It occurs in the dust-bowl areas.

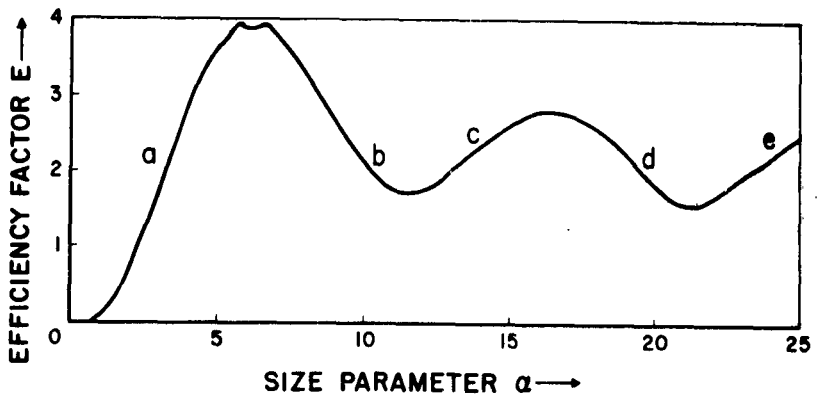

Fig. 1. Schematic representation of the efficiency factor E for extinction as a function of the size parameter α for the refractive index $m = 1.33$ (after Holl and van de Hulst).

d and e will be more or less neutral. In all practical applications, therefore, only parts a and b should be considered and the particle size in question is unique. The next condition to be fulfilled is that the number of particles for which $r \approx \lambda$ must be very large. This can be seen from the following relation. The intensity of solar radiation I_A on a day with anomalous extinction received at the ground is given by

$$I_{A\lambda\zeta} = I_{0\lambda} \exp [-(\beta_\lambda + \gamma_\lambda s) \sec \zeta], \tag{3}$$

where β_λ is the extinction coefficient for wavelength λ by a normal atmosphere and unit air mass; γ_λ the extinction coefficient for wavelength λ by large particles containing N particles/cm³ for a path length of 1 cm; s the vertical thickness of the layer (in cm) and ζ is the zenith distance of the sun.

The absorbed intensity A is then given by

$$A = 1 - I_A$$

and

$$\ln A = -[\ln I_0 - (\beta + \gamma s) \sec \zeta],$$

or putting the constant values together in c_1 and c_2

$$\ln A = [\beta + c_1 N s E(\alpha)] \sec \zeta + c_2. \tag{4}$$

From Eq. (4) it is easily seen that only if

$$c_1 N s E(\alpha) >> \beta,$$

will the extinction in the green and red regions be larger than in the blue. To achieve this, the total number of particles Ns has to be large. An estimate leads to values of 10^7 to 10^8 particles/cm² column, if the proper values for β_λ, as well as $r = 0.5\ \mu$ and $m = 1.33$, are selected for the region 3000 Å to 8000 Å (see Table 5 for numerical values of β). Thus small numbers of particles are unable to reverse the trend of atmospheric extinction as a function of wavelength, and these figures show why the phenomenon is a rare one.

A very instructive graph has been constructed by Foitzik (1950) for γ alone. In Fig. 2 the relative values of γ are plotted as a function of λ for the visible spectrum, assuming that $\gamma s = 1$ for $\lambda = 5500$ Å. For a small radius $r = 0.1\ \mu$, the extinction decreases with wavelength, the factor is about λ^{-3}. This corresponds to part a in Fig. 1. For $r = 0.5$ and $r = 0.6\ \mu$, maximal extinction is found at 5500 Å and 6000 Å, respectively. This corresponds to the first maximum (between parts a and b) in Fig. 1. It will be seen later (Section 4) that particles of this size cause the blue sun phenomenon. Finally $r = 1.0\ \mu$ leads to a

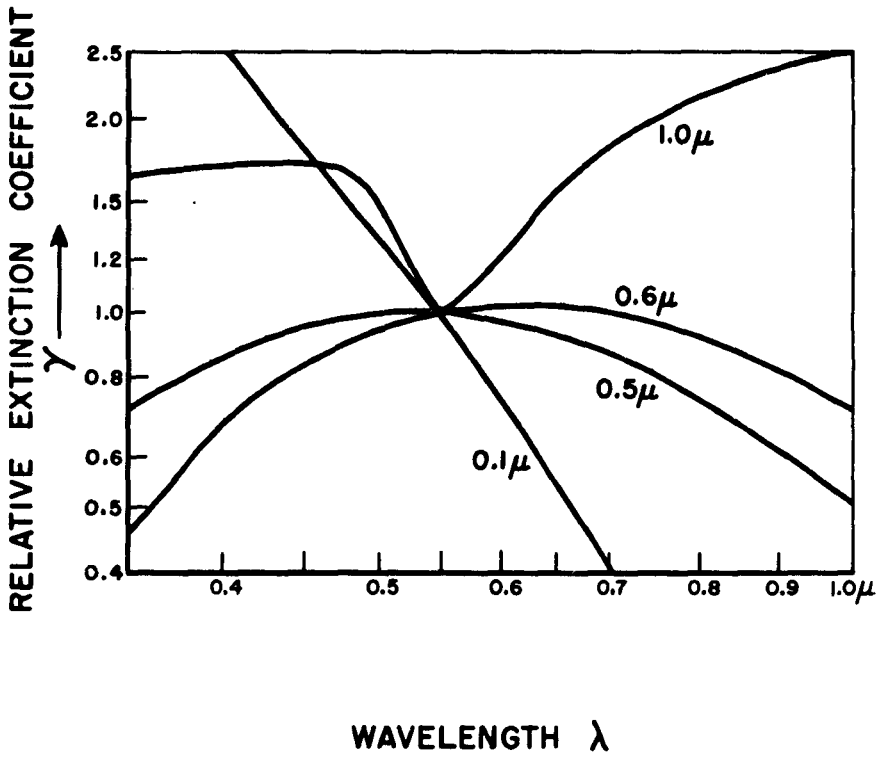

Fig. 2. The relative extinction coefficient γ of water droplets between 3000 Å and 10,000 Å for radii r = 0.1, 0.5, 0.6 and 1.0 μ on a logarithmic scale. The values are plotted so that $\gamma s = 1$ at 5500 Å, the maximum of eye sensitivity.

distinct minimum around 5500 Å, and in this case the sun would look greenish. It corresponds to the minimum between parts b and c in Fig. 1. If the particle size increases to values between $r = 1$ to 1.5 μ, the minimum shifts toward the red and the sun would look reddish. It must be mentioned that this Fig. 2 applies to a uniform size, but the general conclusions are also valid for a size spectrum.

From the foregoing general discussion it can be concluded that a colored sun and moon can be explained on the basis of Mie's theory of large particle scattering, provided that the total number of particles is large, e.g., $> 10^7/cm^2$ column, and the specific color depends on the radius of the particles.

2. OBSERVATIONS OF THE "BLUE" SUN DURING SEPTEMBER 1950

2.1. GENERAL OBSERVATIONS

During September 1950, unusually large forest fires broke out in Alberta and British Columbia, Canada. They reached their peak from 22 to 24 September and generated a tremendous amount of smoke particles. The smoke moved slowly southeast over the continent. But part of it traveled very rapidly across the Atlantic, with an average speed of about 110 to 120 km/hr. Over large parts of Europe, the sun, moon

and stars were seen blue in color between 26 to 30 September. Visual observations (as far east as Poland) are reported in nearly every European meteorological journal. It is not necessary to evaluate each observation here because this will be done by the U. S. Weather Bureau, but to mention only those few facts that are essential for this study.

The bandwidth of the smoke layer was reported as about 1500 km over the eastern United States. The smoke was concentrated over Canada within a band 150 km wide, with a sharp boundary in the north and east edges, thinning out at the south and west edges. The European observations indicate a horizontal spread of about 3000 km or even more. The layer rose to greater heights and grew thicker along its path, indicating an upslide motion as well as horizontal and vertical austausch. The smoke in the eastern United States was largely confined to a layer whose base was near 8000 ft and whose top was at or above 15,000 ft (Wexler, 1950). Over the Atlantic, pilots reported the lower boundary at about 17,000 ft (5.6 km) at 59° N, 25 to 30° W. On 26 September over Leuchars, Scotland, a pilot observed the lower boundary to be at 31,000 ft (9.5 km) and the upper boundary at 43,000 ft (13.1 km). Thus, the thickness of the cloud amounted to about 3.7 km and was situated in the tropopause region (Bull 1951). On 27 September over Cambridge, England, the lower boundary was found to be between 9.1 km and 9.8 km. Pilots flying in the lower part of the cloud reported that the air smelled like burnt paper. This establishes the fact that the particles were smoke particles.

The colors reported in the eastern United States varied very much from place to place, with purple, blue, violet and lavender the most common colors. Observers in Europe, however, reported the physiological impression of a blue sun and a blue moon, of a color comparable to the quartz lamp. The color varied in shade and intensity, and over England one observer saw the moon changing color on the evening of 26 September. At moonrise the color was the normal orange-yellow; it later turned into a sea-green and finally into a blue. Furthermore, a slight color change of sun, moon and stars was observed from time to time after the first appearance, where the blue color was most pronounced, up to 5 and 6 October over Germany. Our conclusion is that all sorts of colors have been seen in the United States, but in Europe only blue was observed. This means that the particle size over Europe was more uniform than over the United States. Color photographs of the blue sun have been taken at the Naval Observatory, Washington, D. C. (unpublished); another one is reproduced by Gebke (1951). No observations of halo or corona around sun and moon are reported, and frequently the absence of such phenomena is stated explicitly. Such observations give a hint that the particle size must have been comparable to, or smaller than, the wavelength of white light.

2.2. SPECIAL OBSERVATIONS

Only three physical measurements of solar radiation through the smoke layer exist.

2.21. *Solar Intensity Measurements By Dietze*

Dietze (1951) measured the total solar radiation, as well as the radiation in the red region, using Schottfilter RG2. The red ratio R ($R = I_R/I_T$, with I_R intensity measured with red filter RG2, and I_T total solar intensity) for this filter is 60 percent for a normal day at the ground. He measured 74 percent indicating a relatively large amount of solar radiation beyond 6250 Å. Dietze concludes correctly from his measurements and from his visual observations that the particle size must have been of the order of the wavelength of white light.

Table 1. Measurements of the solar radiation through the smoke layer at Gotha, Germany (Dietze, 1951) on 28 September 1951.

Time (true local time)	1137 hours
Zenith distance of sun ζ	53°.2
Total intensity of solar radiation I_T	0.29 (ly/min)
Turbidity factor	12.72
True red ratio R	74%
$R - R_0$; R_0 = normal value	7%
Intensity of sky radiation on horizontal surface H	0.42 (ly/min)
H/I_T	2.4

His data as given in Table 1 are very interesting. The total solar radiation amounts to only 0.29 ly/min, the turbidity (in Feussner-Dubois units) to 12.7, which is an extreme value, and the ratio of sky radiation (without sun) H to solar radiation I_T increased to 2.4. The normal value for this zenith distance would be about 0.28 or less. This means that for this turbid atmosphere the radiation from the sky is larger than the direct solar radiation, which is comparable to that of a cloudy day.

2.22. *Extinction Coefficients Measured By Wellmann*

Another valuable measurement has been carried out by Wellmann (1951). He took spectra of the sun between 3800 Å and 4700 Å, using the 2-prism spectrograph and the 1 m-mirror of the Hamburger Sternwarte at Bergedorf, Germany. The dispersion of the spectrograph is given as 40 Å/mm for H_γ. The mirror was dimmed by about 5 m (m = stellar magnitudes). The spectra were taken on 27 September. On 10 October, spectra of the sun were taken in which the general weather situation was similar to that of 27 September, but the smoke layer had definitely disappeared and the color of the sun was normal. The spectra were taken at about the same zenith distances of the sun and it is assumed that the atmospheric transmission on both days was similar, except for the additional extinction caused by the smoke particles on 27 September. Wellmann evaluated his measurements to determine the particle size, but his method was a bit crude. We shall point out in Section 4.2 wherein our calculations deviate. The two sets of data Wellmann took can be used to determine the attenuation of the solar radiation due to the smoke layer.

On a "normal" day, the intensity of the solar radiation I_N received at the ground is given by

$$I_{N\lambda\zeta} = I_{0\lambda} \exp [-\beta_{1\lambda} \sec \zeta]. \tag{5}$$

On the day with the "blue" sun, the intensity of the solar radiation can be expressed as in Eq. (3), i.e.,

$$I_{A\lambda\zeta} = I_{0\lambda} \exp [-(\beta_{2\lambda} \sec \zeta + \gamma_\lambda s \sec \zeta)].$$

If it can be assumed (according to Wellmann's statement) that the atmospheric transmission was the same for both days, $\beta_1 = \beta_2 = \beta$, the ratio

$$\frac{I_{A\lambda\zeta}}{I_{N\lambda\zeta}} = \exp [-\gamma_\lambda s \sec \zeta] \tag{6}$$

gives the transmission due to smoke layer. For further consideration we reduce this ratio for $\zeta = 0$ and write

$$\frac{I_{A\lambda}}{I_{N\lambda}} = e^{-\gamma_\lambda s}. \tag{7}$$

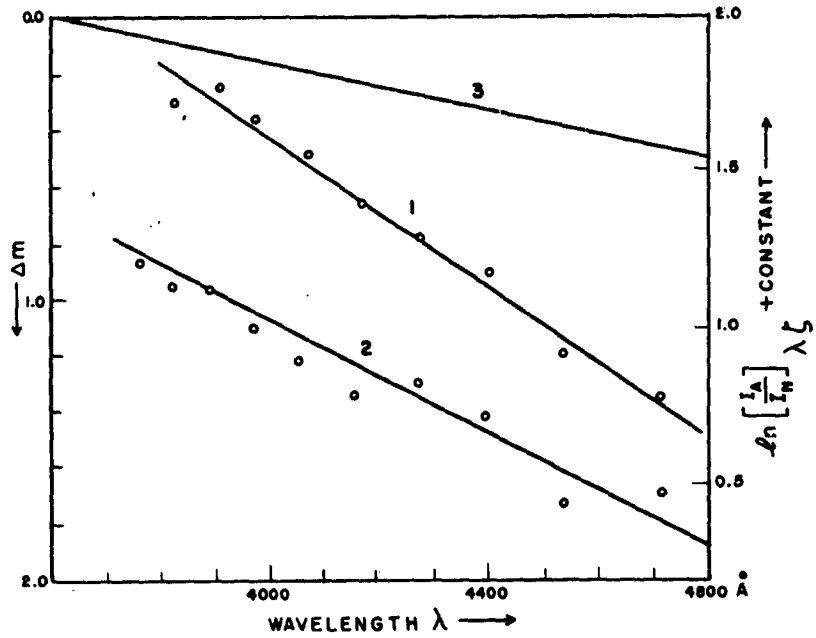

Fig. 3. The anomalous extinction as a function of wavelength according to measurements by Wellmann (Bergedorf, Germany, 27 September 1950).

Curve 1: KS 373 with the points indicating the values found by Wellmann for $\zeta = 67°$.
Curve 2: KS 374 with the points indicating the values found by Wellmann for $\zeta = 61°$.
Curve 3: Reduced values for zenith, $\zeta = 0°$.

Since Wellmann used differences in brightness Δm, and in order to avoid the units of stellar magnitude m, we convert his data by the relation

$$\Delta m = -2.5 \log (I_A/I_N). \tag{8}$$

Since no absolute values have been measured we can write

$$\log (I_A/I_N) = -0.4\, \Delta m + \text{constant}$$

or

$$\ln (I_A/I_N) = -0.921\, \Delta m + \text{constant}. \tag{9}$$

The values Δm are taken from Wellmann's paper and presented in Fig. 3. The ordinate values on the left side are Δm; on the right $\ln(I_A/I_N)$ + constant. Thus, it is seen from the measurements that the observed values can be best approximated by a linear relationship between λ and $\ln(I_A/I_N)$ for the spectral region 2800 Å to 4700 Å. It is not permitted to extrapolate this curve beyond these limits. Curve 3 represents the mean ratio $\ln(I_A/I_N)$ for zenith distance $\zeta = 0$. The numerical values are:

For plate Ks 373: $\ln(I_A/I_N) = \text{constant} - 4.466 \times 10^4\, d\lambda$

For plate Ks 374: $\ln(I_A/I_N) = \text{constant} - 4.680 \times 10^4\, d\lambda$.

Mean value:

$$\ln(I_A/I_N) = \text{constant} - 4.57 \times 10^4\, d\lambda. \tag{10}$$

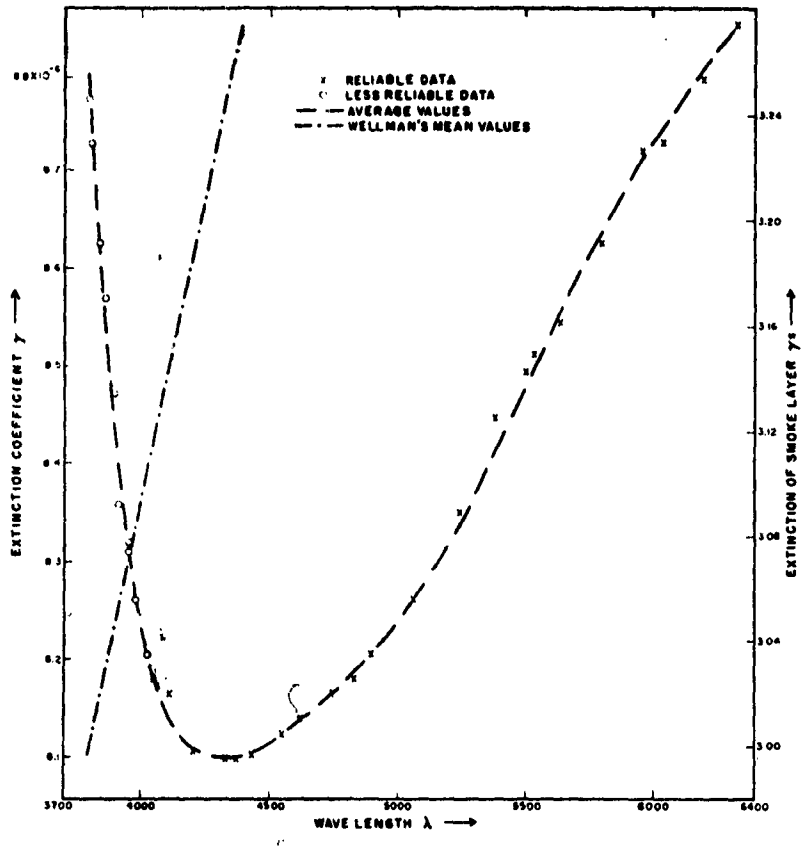

Fig. 4. The anomalous extinction as a function of wavelength according to measurements by Wilson (Edinburgh, Scotland, 26 September 1950).

The difference between the two sets cannot be distinguished on the graph. Thus a mean slope is used in Section 4.3.

2.23. *Extinction Coefficients Measured By Wilson*

The most extensive measurement has been carried out by Wilson (1951). He took spectra between 3811 Å and 6338 Å, using the 36-in. Cassagrin reflector of the Royal Observatory at Edinburgh, Scotland, with the 2-glass prism trained on the attached Hilger universal spectrograph. The dispersion is given as 132, 45 and 28 Å/mm at H_α, H_β and H_γ. The spectra were obtained between 1520 and 1525 GMT on 26 September 1950, at a zenith distance of the sun of 71°. The plates were exposed between gaps in a low cloud deck with exposure times 10, 30 and 180 seconds. Later on the presence of clouds prevented further exposures. Normal sun exposures were obtained on 26 October and 15 November 1950, with a zenith distance of the sun of 69° and 73°, respectively. The formalism of the preceding section can also be applied to Wilson's observation, since he uses stellar magnitudes. The extinction coefficient of the smoke layer for vertical incidence is given by

$$\gamma_\lambda = \frac{0.921}{s \sec \zeta} \Delta m_\lambda,$$

which follows from Eqs. (7) and (8). The results for $\gamma_\lambda s$ are represented in Fig. 4. Between 6338 Å and

4028 Å, Wilson considers the values consistent and reliable (crosses in Fig. 4). Below 4028 Å, less weight should be given to the numerical values (open circles in Fig. 4) because they cover a spectral range that was never meant to be utilized in the instrument employed (instrumental absorption, spectrum no longer in sharp focus and other reasons are listed by Wilson). A mean curve has been drawn through the experimental points. The extinction coefficients show a pronounced minimum around 4300 Å, which falls within the range considered reliable. The extinction increases toward the ultraviolet and green parts of the spectrum; however, the increase toward the ultraviolet is too steep. As can be seen from the figure, Wellmann's extinction coefficients are different, indicating that the particle size was different for both observations.

Wilson also evaluated his data and his method will be explained later in Section 4.2.

3. CHEMICAL COMPOSITION OF SMOKE PARTICLES

Samples from the smoke layer have not been analyzed, but only two possibilities exist regarding the composition of the particles.

(a) They consist of nearly pure carbon coated with water or ice.

(b) They consist of organic compounds, especially wood oil (suggested by Elsley (1951)).

Let us consider the first alternative. Tiny soot particles have definitely been produced in large quantities. Because they are hygroscopic and because they traveled several days in the troposphere, the surface is wet.* Over Europe the temperature of the layer was around $-50°$ to $-60°$C and therefore the outer film consists of ice.† Thus, it seems fairly certain that the soot particles are covered with an ice film, the thickness of which is unknown.

The second alternative is that the particles consist of a complex mixture of oils (wood oils) which are always produced in such a combustion process, together with wood creosote and some carbolic acid or phenols. The oils leave the fire area in a gaseous phase, condense in the atmosphere, coagulate and later on — in the cold upper troposphere — may be solidified.** Since these oils are not solvent, coating with ice or water is not possible. Because they are volatile, they may produce the odor of burning wood which has been noticed by the pilots. Elsley states that airplanes flying through the smoke layer in the Great Lakes region "were found to be covered with a thin film of a pale brown, oily smelling substance, that was probably a resinous distillate." Unfortunately this deposit has not been analyzed chemically. This fact also points very strongly to the second alternative. After the particles become solid, coagulation ceases and particle size remains more or less constant. This fact seems to explain the various colors observed in the United States, where the size of these liquid droplets varied with time and place, and the more or less uniform blue color observed over Europe, where the particles were solidified and changed very little in size.

From this discussion it seems fairly certain to me that the cloud consisted mainly of solid oil particles.

---

* In an atmosphere where the relative humidity is ≥ 70 percent, practically all particles possess a droplet character. It seems certain to me that the amount of water vapor in the troposphere has been sufficient to wet the surface of the particles.

† The lowest freezing temperature of supercooled water droplets in the atmosphere is given as about $-40°$C.

** It is possible to supercool such oil droplets, but the temperatures at which this occurs are unknown.

4. RADIUS AND CONCENTRATIONS OF SMOKE PARTICLES

4.1. THEORETICAL CALCULATIONS

In order to evaluate Wellmann's and Wilson's measurements, the variables as well as the constant factors are carefully selected. Some are not properly known. Therefore, the errors due to such an uncertainty are studied in detail. The factors are:

(a) The size spectrum; two cases will be considered in Sections 4.11 and 4.12.

(b) Because the smoke particles are probably wood oil, the refractive index will be $m \approx 1.46$, at any rate $1.25 < m < 2.0$. The numerical calculations will be carried out for $m = 1.33$, solely because the efficiency factor E is best known for this value of m. This question will be thoroughly discussed in Section 4.13.

(c) A spherical shape will be assumed, because E is best known for this shape. It will be shown in Section 4.14 that the shape factor does not alter the results remarkably.

(d) In calculating N, the thickness of the layer is assumed to be $s = 3.7$ km, according to the pilot observations over Scotland (Bull 1951). Moreover, it is assumed that the particles are evenly distributed within the layer. These two assumptions enter only into the calculation of N. The total amount N_T, independent of this assumption, will be used for all further calculation in Sections 5 and 6.

4.11. *Uniform Size*

As a first approximation, it is assumed that all particles possess a uniform size, with radius r. They have uniform refractive index m and are spheres.

From Eq. (10), it follows, after differentiating with respect to λ, that

$$\frac{d\,[\ln\,(I_A/I_N)]}{d\lambda} = -0.457 \times 10^5 \tag{12}$$

and Eq. (7), it follows that

$$\frac{d\,[\ln\,(I_A/I_N)]}{d\lambda} = -s(d\gamma/d\lambda). \tag{13}$$

The left-hand side of Eqs. (12) and (13) are equal, thus

$$d\gamma/d\lambda = 0.457 \times 10^5 \cdot \frac{1}{s}$$

and with $s = 3.7 \times 10^5$ cm

$$d\gamma/d\lambda = 0.1235 \left[\frac{1}{\text{cm}}\right]. \tag{14a}$$

Later on we like to use the wave number n instead of λ thus

$$d\gamma/dn = -\frac{0.1235}{n^2}. \tag{14b}$$

The extinction coefficient γ is defined by the Mie theory (Eq. (1)) in Section 1. Differentiating Eq. (1) with respect to n,

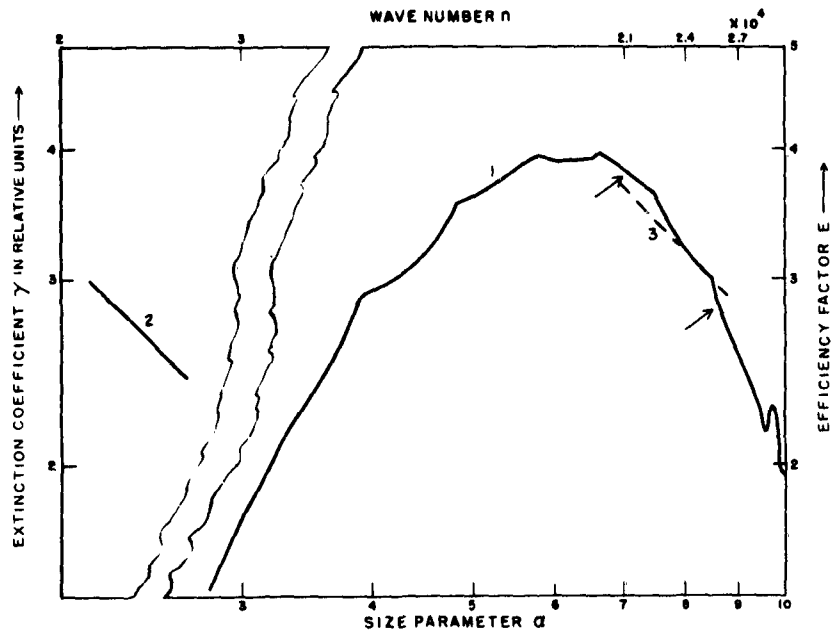

Fig. 5. The efficiency factor E as a function of the size parameter α for $m = 4/3$ (after Holl) in logarithmic scale, for case 1. The function E is represented only between $\alpha = 2.8$ and 10 (curve 1). The straight line (curve 2) on the left represents the measured values of γ as a function of n (after Wellmann) for the region 3800 Å to 4700 Å, also in logarithmic scale. (γ in a relative scale, because only the gradient $d\gamma/dn$ is actually measured.) The best fit of Wellmann's data with the theoretical curve is given as a dashed line (curve 3); the arrows indicate the limits of Wellmann's data.

$$d\gamma/dn = \pi r^2 N \frac{dE(\alpha)}{dn} = 2\pi^2 r^3 N \, dE/d\alpha. \tag{15}$$

Taking the logarithms on both sides

$$\ln (d\gamma/dn) = \ln(dE/d\alpha) + \ln (2\pi^2 r^3 N) = \ln (dE/d\alpha) + \text{constant}. \tag{16}$$

Because r and N are regarded as constant within the layer, the second term is a constant. Furthermore, for a given λ the logarithms of the gradients are equal except for this additional constant which is independent of λ. This expression (Eq. (16)) allows the calculation of r in a very simple way. If $d\gamma/dn$ is known experimentally (in our case for the region 3800 Å to 4700 Å by Eq. (10)), and if $dE/d\alpha$ is known from theoretical calculations for the specific value of m, then these two gradients can be compared by a simple graphical method suggested to me by E. Inn. On one logarithmic graph paper γ is plotted as a function of m; on another, E is plotted as a function of α. Thus the logarithms of the gradients $d\gamma/dn$ and $dE/d\alpha$ are known over a certain range of n and α. Both graph papers are now superimposed and the best agreement of both curves found, then this position of the two papers is fixed. A certain value of n corresponds to a certain value of α, this can be seen easily on Fig. 5, which is a composite figure of the two graph papers. For example, for $\alpha = 8$, $n = 2.4 \times 10^4$.

Unfortunately for our case, Wellmann measured $d\gamma/dn$ only for a small region of n. For a first approximation, however, it is sufficient to find α values to corresponding values of n. The better approximation was carried out numerically by calculating $d\gamma/dn$ and $dE/d\alpha$ for 10 points and the final determination of

corresponding values of α and n was based on the best agreement of Eq. (16). The radius r is found from Eq. (2) by inserting the values α and n obtained by the procedure just described.

Having found r, the next step is to calculate N from Eq. (15)

$$N = \frac{1}{2\pi^2 r^3}\left(\frac{d\gamma}{dn}\right)\frac{1}{(dE/d\alpha)}, \tag{17a}$$

or in our particular case, using γ for the region 3800 Å to 4700 Å as measured by Wellmann we get, using Eq. (14b),

$$N = -\frac{0.247}{\alpha^2 r}\frac{d\alpha}{dE}. \tag{17b}$$

Since $d\alpha/dE$ is negative in the region, N is a positive value.

4.12. *Size Spectrum*

The last chapter refers to smoke particles of uniform size. This is certainly only a first approximation, because the particles generated by a forest fire will spread over a more or less extended size range. Since the smoke traveled several thousands of miles from Canada to Europe, it is understandable that the size spectrum within a vertical column of the smoke layer became narrower with increasing distance from the source. The size spectrum will probably vary in a horizontal direction along the smoke layer, as indicated by the various colors observed in the United States (Wexler 1950). But if measurements like Wellmann's are carried out, one is confronted with a size distribution within a column at a given instant. It seems very probable to represent it by a Gaussian distribution, because the layer consists of particles of the same chemical composition.*

The Gauss error function is

$$y = \frac{h}{\sqrt{\pi}} e^{-h^2x^2}, \tag{18}$$

where h is the precision measure (indicating the steepness of the function). This can be normalized by $u = hx$

$$y = \frac{h}{\sqrt{\pi}} e^{-u^2} = h\phi(u), \tag{19}$$

where

$$\phi(u) = \frac{1}{\sqrt{\pi}} e^{-u^2}.$$

If the distribution of particles is considered it can be written as

$$N_r = Ch\phi(u) = C\frac{h}{\sqrt{\pi}} \exp\left[-h^2 \log (r/r_0)^2\right] \tag{20}$$

where C is an arbitrary constant, instead of as in Eq. (19). The quantity N_{r_0} is the ordinate at the peak,

* A comparison of the expected distribution can be made with distribution functions obtained from electron microscope pictures of soot particles from flames (Pepperhoff 1951) which show a very distinct Gaussian distribution. No comparison should be made with distribution functions of dust particles, however, because "atmospheric" dust consists of particles of different chemical composition and different origin. They are inhomogeneous in every respect and this leads to very irregular distribution functions. Gaussian distribution functions have also been obtained for raindrop-size spectra, which are homogeneous particles in the sense just used.

$$N_r = N_{r_0} \exp [- h^2 \log (r/r_0)^2].$$

The total number of particles to be found in 1 cm² is then

$$N_M = \int_0^\infty N_r \frac{dr}{r} = \int_{-\infty}^\infty N_r \, d(\ln r). \tag{21}$$

Putting Eq. (20) into Eq. (21) yields

$$N_M = N_{r_0} \int_{-\infty}^{+\infty} \exp [- h^2 \log (r/r_0)^2 \, d(\ln r)],$$

with

$$u = h \log (r/r_0).$$

It follows that

$$N_M = N_{r_0} \frac{\sqrt{\pi}}{h \log e} \frac{1}{\sqrt{\pi}} \int_{-\infty}^{+\infty} e^{-u^2} du = \frac{N_{r_0} \sqrt{\pi}}{h \log e}, \tag{22}$$

because

$$\int_{-\infty}^{+\infty} \phi(u) du = 1.$$

The efficiency factor E_M for a size spectrum can be defined and it has been defined by several workers in this field. Since we shall use the numerical values of E_M calculated by Foitzik, we shall follow his derivation.

The extinction coefficient γ was defined by Eq. (1) for a uniform size r

$$\gamma_{r\lambda} = \pi r^2 N_r E(\alpha) = \frac{\alpha^2}{4\pi n^2} N_r E(\alpha).$$

For a size spectrum it is

$$\gamma_{M\lambda} = \sum \gamma_{r\lambda} = \frac{1}{4\pi n^2} \int_\alpha \alpha^2 N_r E(\alpha) d\alpha. \tag{23}$$

Let us now define a new efficiency factor $E_M(\alpha)$ for a size spectrum following Foitzik's definition (1950),

$$\gamma_{M\lambda} = \frac{\alpha^2}{4\pi n^2} N_M E_M(\alpha). \tag{24}$$

We use $\gamma_{M\lambda}$ from Eqs. (23) and (24) and find that

$$\int_\alpha \alpha^2 N_r E(\alpha) d\alpha = \alpha^2 N_M E_M(\alpha),$$

or with N_M from Eq. (21)

$$\int_\alpha \alpha^2 N_r E(\alpha) d\alpha = \alpha^2 E_M(\alpha) \int_r N_r \, d(\ln r).$$

Dividing both sides by N_{r_0} yields $N_r/N_{r_0} = y$, i.e., Eq. (18),

$$\int_\alpha \alpha^2 y E(\alpha) d\alpha = \alpha^2 E_M(\alpha) \int_r y \, d(\ln r).$$

Thus

$$E_M(\alpha) = \frac{1}{\alpha^2} \frac{\int_\alpha \alpha^2 y E(\alpha) d\alpha}{\int_r y \, d(\ln r)}. \tag{25}$$

Foitzik calculated $E_M(\alpha)$ for a refractive index $m = 1.33$ and for three values of h — namely, $h_1 = 7.07$, $h_2 = 5.196$, $h_3 = 3.873$ — which correspond to the standard deviation $\sigma_1 = 0.1$, $\sigma_2 = 0.136$ and $\sigma_3 = 0.182$.

Unfortunately, he used Stratton-Houghton's value for $E(\alpha)$, instead of Holl's or Houghton-Chalker's (1949) which are better. For a first approximation, however, both $E(\alpha)$'s agree, but beyond the second maximum Stratton-Houghton's values are unreliable.

This definition of $\gamma_{M\lambda}$ and $E_M(\alpha)$ allows the calculation of r_0 and N_M by inserting them instead of γ and E into Eq. (16). The procedure to obtain values for r_0 and N_M is analogous to the procedure described in the last section.

4.13. *Refractive Indices* $1.25 < m < 2.0$

Since the refractive index $m = 1.33$ — i.e., the refractive index for water droplets — was used, the question arises whether or not this is a good approach. The refraction index m of the particles is unknown, but may be estimated for the two kinds of particles discussed in Section 3.

For amorphous carbon m is relatively high, i.e., $m = 1.97$; for water it is 1.33; for ice it is nearly the same, i.e., $m = 1.30$, and for ice at very low temperatures it drops to $m = 1.25$. If the particles consist of two spheres of different refractive indices — e.g., the inner core with $m = 1.97$, the outer sphere with $m = 1.25$ — only the refractive index of the outer sphere has to be considered, provided that the outer sphere has a certain depth. The numerical value is not known for this case but can be judged as probably 10^{-2} to 10^{-4} of the total radius to be sufficient.* Thus, it is concluded that for this case m will be close to that of ice, say around $m = 1.3$, and the results differ only slightly from those obtained for $m = 1.33$, for which case the calculations are carried out.

Let us turn now to the second alternative mentioned in Section 3. For a mixture of wood oils the refractive index depends on the substances, but they all have practically the same value. The range is about $m = 1.45$ to 1.47, and a mean value of $m = 1.46$ is perhaps reasonable. Thus it is estimated that the chosen value $m = 1.33$ is not far from the true value. Table 2 shows the various values which might be appropriate.

The $m \ll 2$ is clearly demonstrated by Wellmann's data. Namely, if the particles are uncoated they should absorb strongly. For such particles the fluctuation of the E function beyond the first maximum becomes less pronounced and it would mean a more or less neutral extinction, which is not observed. Thus, this points very strongly to the chosen value of m.

The value $m = \infty$, often ascribed to dust, is impossible according to the foregoing reasons for m. Moreover, it is excluded because the extinction would be constant after the first maximum. Wellmann

---

* Aden and Kerker (1951) have shown that, for a particle with an ice core and a water sphere surrounding it, a thickness of the water film one-fifth of the total radius or more is sufficient to have the same reflectivity as a pure water particle, if the wavelength $\lambda = 10$ cm is used. The wavelength of the radiation is 2×10^5 higher in their case than in our case. Therefore, a smaller thickness will give the same effect.

Table 2. Values of refractive indices (for Sodium D-lines).

	m
Ice at very low temperature	1.25
Ice at 0°C	1.31
Water	1.33
Wood oil	1.46
Quartz	1.55
Coal, amorphous	1.97

argued against $m = \infty$ only from the point of neutral extinction, but the actual values of m, as discussed above, are already the best argument why such a value can never be considered.

It has been shown by van de Hulst (1949) that for $1 < m < 2$ the curves E against $\alpha(m-1)$ are very similar and for values of m closely related, the E values are identical, for all practical purposes, provided that the parameter $\alpha(m-1)$ is used instead of α. Thus the E value is the same for all $\alpha(m-1)$ if m varies between 1 and 2. We may write

$$E[\alpha(m-1)] = E[\alpha_w(m_w-1)],$$

or, if E is constant,

$$\alpha(m-1) = \alpha_w(m_w-1). \tag{26}$$

The index w denotes the values for water droplets. If Eq. (2) is inserted,

$$r = r_w\left(\frac{m_w-1}{m-1}\right). \tag{27}$$

This applies to the uniform size as well as for a size distribution. That means that only one set of E values for a particular m has to be calculated and the corresponding values $E(\alpha)$ for another m can be obtained by a simple transformation. This applied to E as given by Holl and to E_M as given by Foitzik. The value N changes, also. From Eq. (17a) it follows with

$$d\alpha = d\alpha_w\left(\frac{m_w-1}{m-1}\right)$$

from Eq. (26), that

$$N = N_w\left(\frac{m-1}{m_w-1}\right)^2 \tag{28}$$

where

$$N_w = \frac{1}{2\pi^2 r_w^3}\left(\frac{d\gamma}{dn}\right)\left(\frac{d\alpha_w}{dE}\right).$$

But if Eq. (28) is inserted into Eq. (1) it follows that

$$\gamma = \pi r^2 N E[\alpha(m-1)] = \pi r_w^2 N_w E[\alpha_w(m_w-1)] \tag{29}$$

remains unchanged whatever value of m is used. This also has a very important effect on our calculations. We shall get other values for r and N (see Table 3) for a given experimental set of γ_λ, but all calculations using γ — i.e., Sections 5 and 6 — remain unaltered whatever refractive index is provided ($1.25 < m < 2$).

Table 3. Values of r and N as functions of m.
Relative values r/r_w and N/N_w are calculated, using m_w as standard.

m	1.25	1.31	1.33	1.46	1.55	2
r/r_w	1.32	1.06	1	0.72	0.60	0.33
N/N_w	0.57	0.88	1	1.94	2.79	9.00

4.14. *Anisotropic Particles*

It has been assumed that the particles are spherical. It is realized, however, that this may not be the actual case. From theoretical calculation Gans concluded that the anisotropy is of very minor influence as long as the refraction index is small, i.e., $m < 2$ (see Linke 1942, p. 213). The values of E will change very little, not exceeding 10 percent. Van de Hulst calculated an increase of 6 percent for cylinders with $m = 1.25$ and $m = 1.50$.

The increase in intensity is, of course, not so easy to determine, because the increase occurs in the exponent of Eq. (3), but from a few numerical calculations the author is convinced that the influence is of very minor importance, regarding the other uncertainties like size spectrum and m.

4.15. *Thickness of Layer*

Whereas the thickness of the smoke layer along its path was not uniform, as can be concluded from the observations on the ground, the altitude range and the order of magnitude, as found by the pilot over Scotland (Bull 1951), will not have changed on its way from Scotland to Hamburg.

The total number of smoke particles $N_T = Ns$ is obtained directly from Wellmann's measurements and this value alone is the important factor entering all calculations. The factor N, however, is calculated to indicate the average concentration if $s = 3.7$ km. Moreover, N is certainly smaller at the lower and upper boundary of the layer than within, but no estimate of the vertical distribution of N can be given.

4.2. WELLMANN'S AND WILSON'S METHODS

Wellmann's determination of r differs from ours. He used only the slope of the extinction coefficient $d\gamma/dn$ and determined the point where the tangent to the curve $E(\alpha)$ has the same slope, namely, $d\gamma/dn = dE/d\alpha$. Since the function $E(\alpha)$ is not linear, his method will yield only a first approximation. We shall see in the next section that his approximation is fairly good.

Wilson used another method. He obviously could not fit his data to an extinction caused by particles of uniform size. Therefore, he assumed that an overall reddening takes place in the atmosphere, and he represents this by an $(1/\lambda)^x$ law. Thus, he wrote the extinction coefficient

$$\gamma = \frac{1}{s}\left\{\pi r^2 NE + p\left(\frac{1}{\lambda}\right)^4\right\}. \tag{30}$$

The first factor is the usual extinction by large particles (see our formula Eq. (1)), the second term corrects for what he calls atmospheric reddening.

Computations are carried out by trial and error to obtain the best fit for all observations and for those between 4028 Å and 6338 Å. No fit could be obtained for all observations, but a good fit was obtained for this limited range. The numerical values obtained are

$$\gamma s = \frac{0.71}{2.5 \log e}\left\{E + 1.51 \times 10^{-4}[2\alpha(m-1)]^4\right\}. \tag{31}$$

From $2\alpha(m-1)$, r is calculated according to Eq. (2) and the total number from the constant factor in Eq. (31)

$$0.71 = \pi r^2 N_T.$$

The computed values agree approximately with our results (see Table 4). The assumption of an overall reddening, however, cannot be easily explained and he does not attempt to verify it. This factor is similar to the Rayleigh scattering, decreasing rapidly with increasing wavelength. This extinction could be caused only by particles smaller than $1/10\,\lambda$, say $r \leq 0.05\,\mu$. They must be a characteristic part of the smoke layer and be extremely numerous. There is nothing known to substantiate his assumption, and I think it is much more conceivable to explain his data by a size distribution of the particles, instead of the uniform size which he assumes.

4.3. NUMERICAL CALCULATIONS AND DISCUSSION OF RESULTS

The methods described above in principle have been employed to Wellmann's and Wilson's data. The following two cases will be considered: case 1, dealing with a uniform size follows from Section 4.11 and cases 2 and 3, with a Gaussian distribution of the size spectrum as explained in Section 4.12.

In Fig. 5, E is plotted as a function of α in a logarithmic scale, according to the best theoretical values calculated by Holl (1948). In the same figure γ is plotted as a function of n in the spectral region measured (curve 2), also in a logarithmic scale. In such a coordinate system $d\gamma/dn$ is then a straight line. It is obviously seen that only a small part of the corresponding $E(\alpha)$ can be compared with $\gamma(n)$.

The only region where a good fit can be accomplished is between $\alpha = 6.7$ and $\alpha = 9.6$. The slope of $E(\alpha)$ beyond the second maximum at $\alpha \backsim 16$ and any following maximum (see Fig. 1) is too steep and has to be excluded, because no good fit can be found for Wellmann's data. The best fit is indicated by curve 3, which has been obtained by the method described in Section 4.11. For this fit $d\gamma/dn = -0.15$, whereas Wellmann observed -0.12. The numerical results are given in Table 4 (a).

For case 2 the best fit has been obtained with E_M using $h = 7.07$ or a standard deviation of $\sigma = 0.1$. Higher standard deviations gave E_M functions which are much flatter after the first maximum, the largest gradient was -0.6 and -0.38, instead of -1.0 as required by Wellmann's observation. This fit is much better than in case 1, as can be seen from Fig. 6.

The numerical results as published in Table 4 (a) are in one sense surprising. The rough comparison of the slope, which Wellmann carried out, already leads to the correct order of magnitude for r and N_T. The differences between cases 1 and 2 are minor. Whereas r increases only by 1 percent, N increases by about 25 percent. This means that r can be calculated very exactly by simple assumptions.

Table 4. Radius, total number and number density of smoke particles.

(a) For $m = 4/3$

Place	Hamburg			Edinburgh	
Author	Wellmann	Penndorf		Wilson	Penndorf Case 3
		Case 1	Case 2		
Radius r_0 in μ	0.53	0.522	0.528	0.785	0.820
Total number of smoke particles N_T/cm² column	7.5×10^7	5.2×10^7	6.5×10^7	....	4.7×10^7
Number density of smoke particles N (1/cm³)	....	140	175	....	127

(b) For $1.10 < m < 2.0$

m		Hamburg			Edinburgh	
		Wellmann	Penndorf		Wilson	Penndorf Case 3
			Case 1	Case 2		
1.10	r_0	....	....	....	2.60	....
1.25	r_0	....	0.687	0.660	1.04	1.08
	N_T	....	3.0×10^7	3.7×10^7	....	2.68×10^7
1.31	r_0	....	0.553	0.560	....	0.87
	N_T	....	4.6×10^7	5.7×10^7	....	4.14×10^7
1.46	r_0	....	0.375	0.380	....	0.59
	N_T	....	1.01×10^8	1.26×10^8	....	9.12×10^7
1.50	r_0	....	....	....	0.52	0.54
	N_T	....	....	....	2.7×10^7	1.08×10^8
1.55	r_0	....	0.313	0.317	....	0.49
	N_T	....	1.45×10^8	1.81×10^8	....	1.31×10^8
2.0	r_0	0.2	0.172	0.174	0.26	0.27
	N_T	6.0×10^8	5.2×10^8	5.8×10^8	....	4.23×10^8

Note: Case 1 = uniform size; case 2 and case 3 = Gaussian distribution of size spectrum.

Wilson's measurements cover a much wider spectral range than Wellmann's, even if the data below 4028 Å are excluded (see Section 2.23). If we treat those data, no fit can be accomplished with the efficiency factors E for uniform size. However, they fit the efficiency factors for a narrower size distribution than Wellmann's very well, i.e., for a size distribution with $\sigma = 0.136$ (case 3). This can be seen from Fig. 7, where the experimental curve d agrees with curve b. The abscissas for both curves are so arranged that they

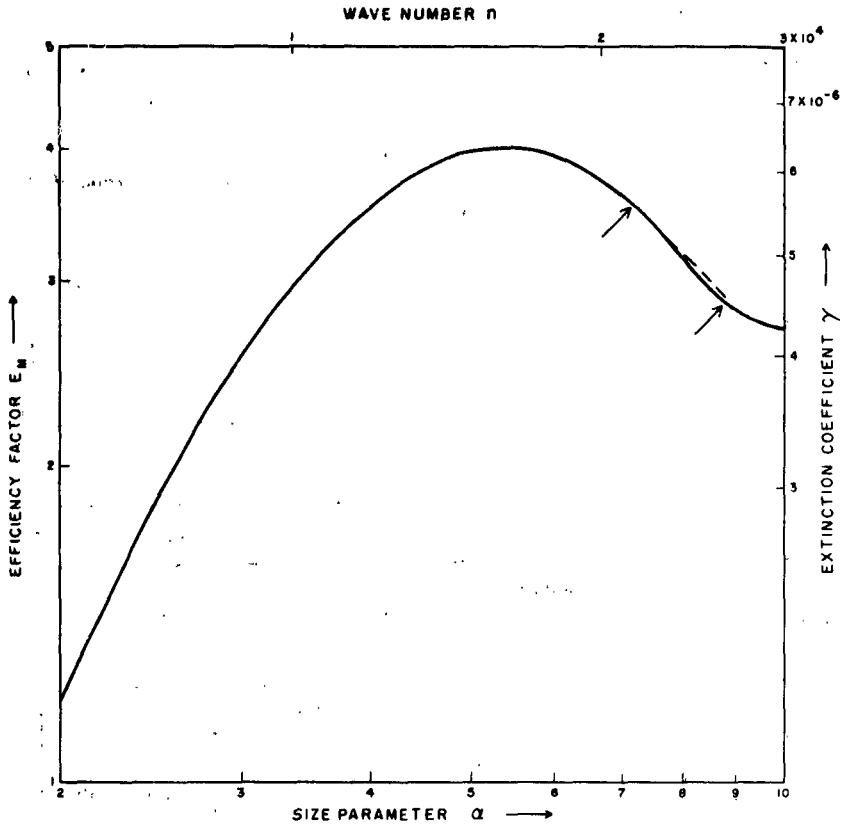

Fig. 6. The efficiency factor E_M as a function of the size parameter α for $m = 4/3$ in a logarithmic scale (after Foitzik) for a particle size distribution for case 2. The function E is represented only for α between 2 and 10. The best fit of Wellmann's data is shown as a dashed line; the arrows indicate the limits of his data.

correspond to the best fit. Foitzik's curve for $\alpha > 12$ is probably too flat; there should be a slight secondary maximum around $\alpha = 13$ or 14.

This solution seems to me more satisfactory than Wilson's assumption of a uniform size plus a general extinction according to a λ^{-4} law, which has never been found otherwise in such studies. It seems much more realistic to assume a size spectrum to explain his data.

The results of the calculation are contained in Table 4. The radius $r_0 = 0.820\ \mu$, a value which is a little higher than Wilson's. The total number of particles N_T is 4.7×10^7, which is an order of magnitude higher than Wilson's, because he assumed the additional small particles. A comparison of both observations reveals that some significant discrepancies exist. Although the number of particles — comparing cases 2 and 3 — are about equal, the particle sizes are not.

The actual size distribution for cases 2 and 3 has been plotted (Fig. 8) according to Eq. (20). It is easily seen that over Hamburg the smaller particles are much more numerous than over Edinburgh. Between $r_0 \pm 0.05\ \mu$, 31 percent of the total number are found over Hamburg, but only 15 percent over Edinburgh. It is safe to say that practically all particles over Hamburg are found between 0.3 and 0.9 μ and between 0.5 and 1.3 μ over Edinburgh.

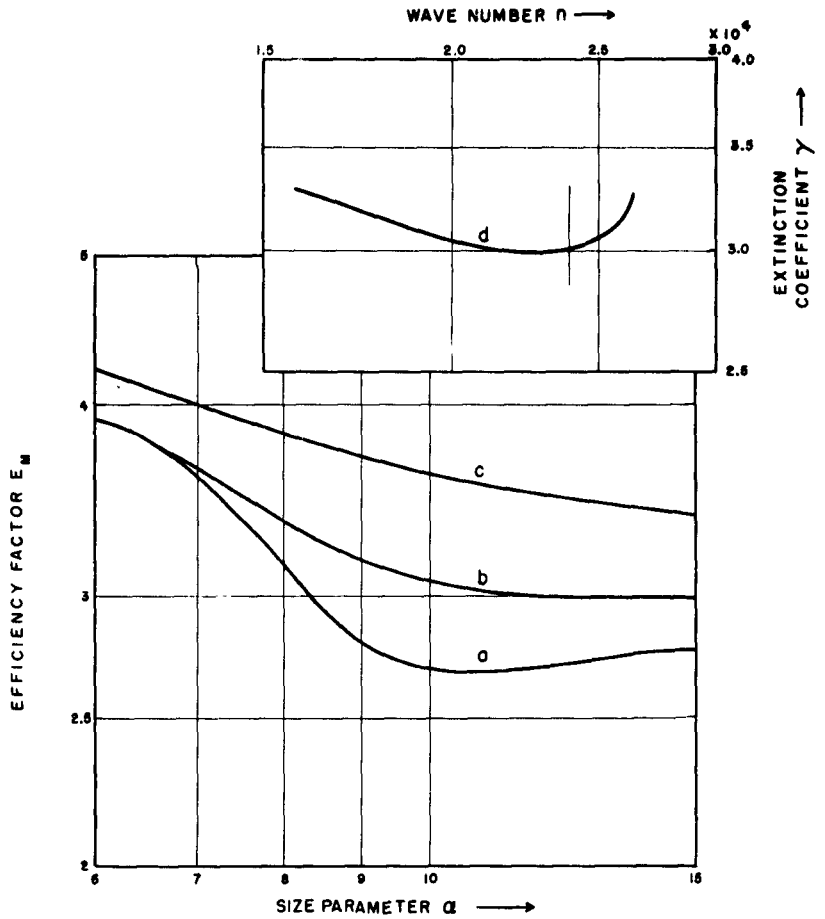

Fig. 7. The efficiency factor E_M as a function of the size parameter for $m = 4/3$ in a logarithmic scale (after Foitzik) for case 3. Curve a for $h = 7.07$; curve b for $h = 5.20$; curve c for $h = 3.87$. Curve d: measured extinction coefficient (in relative scale) as a function of wave number n (after Wilson). The data between $n = 2.4$ and 2.6 are considered less reliable by the author (Wilson). Curve d (between $n = 1.6$ and 2.4) matches curve b best, but does not match any of the others.

It is very hard to draw further conclusion, because both observations are based more or less on one exposure taken at a distinct time. If a series of exposures had been taken, perhaps a change with time of the size distribution may have been observed.

If $m = 4/3$ is not the appropriate value for the refractive index, Table 4 (b) shows the numerical results according to Table 3 (Section 4.13). Under the headings "Wellmann" and "Wilson," the values given in their publication have been entered. Under the heading "Penndorf," those calculated according to Table 3 are given. For ice particles at very low temperature ($m = 1.25$), r_0 is much larger, namely, 0.660 μ over Hamburg and 1.08 μ over Edinburgh, but the total numbers are smaller. If $m = 1.46$, namely for wood oils, $r_0 = 0.380\ \mu$ over Hamburg and 0.59 μ over Edinburgh and the total number is about $10^8/cm^2$ column. Higher values of m are unlikely but the numerical values are given. The effect of anisotropy of the particles will alter r_0 only by a few percent and is insignificant in comparison to other uncertainties.

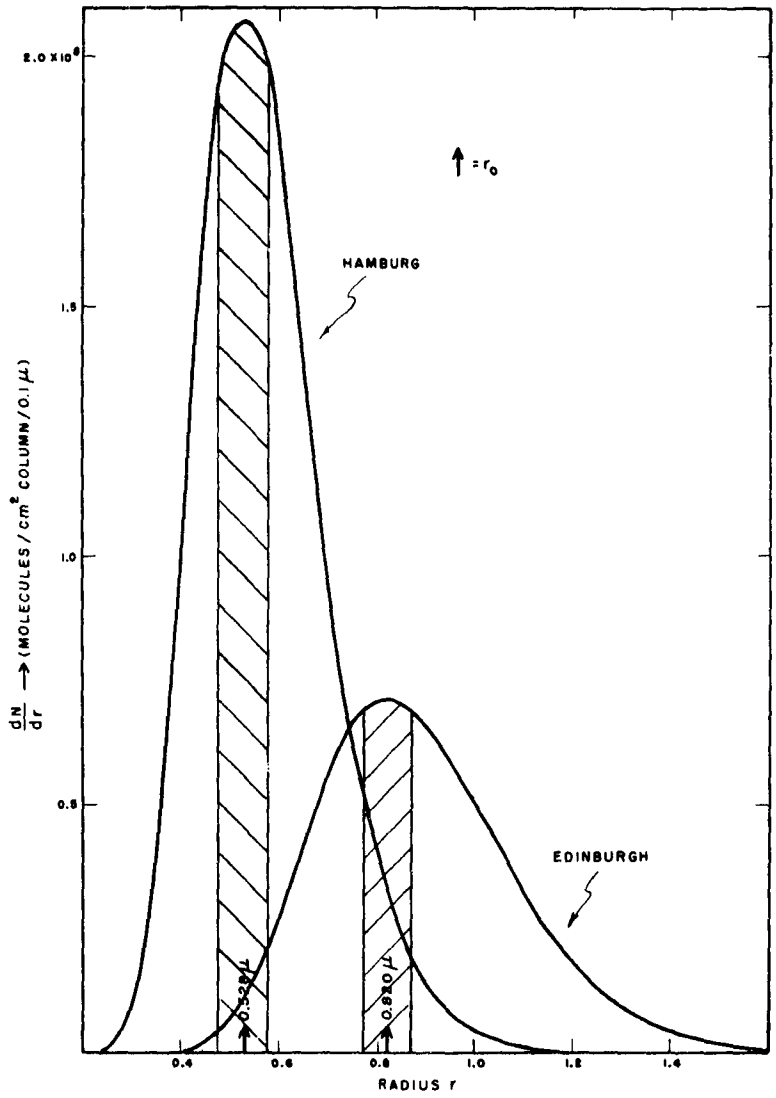

Fig. 8. Size distribution for cases 2 and 3 and $m = 4/3$. The ordinate gives the number of particles N contained within a radius range of 0.1 μ. The shaded area shows the number of particles contained in the range $r_0 \pm 0.05$ μ.

In general, it can be stated that at that particular time the radius r_0 was between 0.38 μ and 0.66 μ over Hamburg with a total number N_T between 3.7×10^7 and 1.26×10^8/cm² column, whereas over Edinburgh the numbers for r_0 are 0.59 μ and 1.08 μ and N_T between 2.68 and 9.12×10^7/cm² column. Furthermore, there existed a spread over a size range which changes with respect to the m selected, but the character of Fig. 8 for $m = 4/3$ will remain.

5. ANOMALOUS EXTINCTION BETWEEN 3500 Å AND 7000 Å FOR SEPTEMBER 1950

Now the numerical values of the extinction on 27 September 1950 can be calculated. The extinction of the normal air β is taken from Linke (1942, p. 249) for a clear day. It contains the extinction due to molecular scattering, scattering by large particles which contaminate the air on a "normal clear" day and absorption

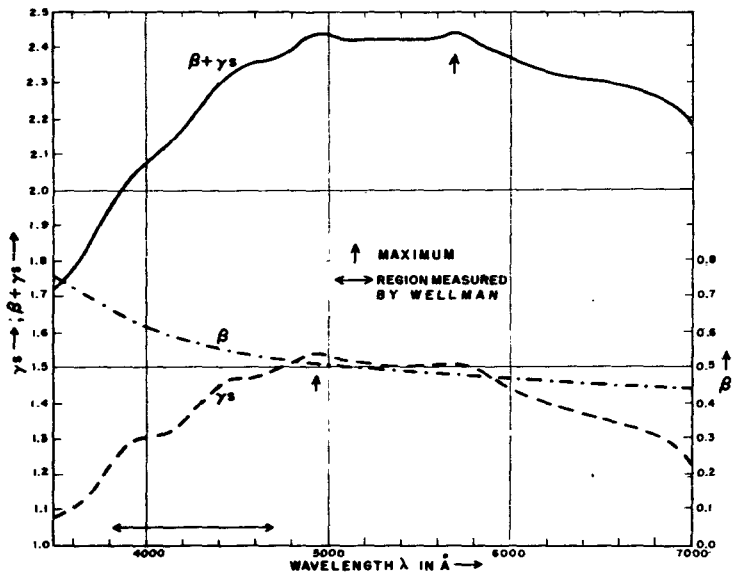

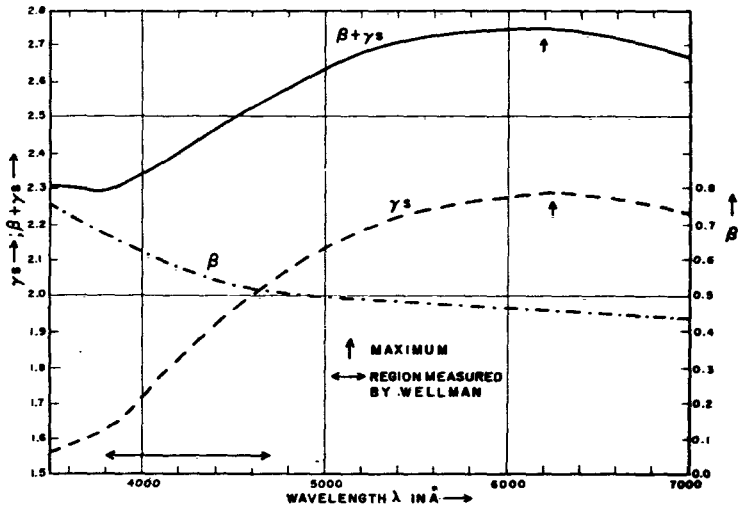

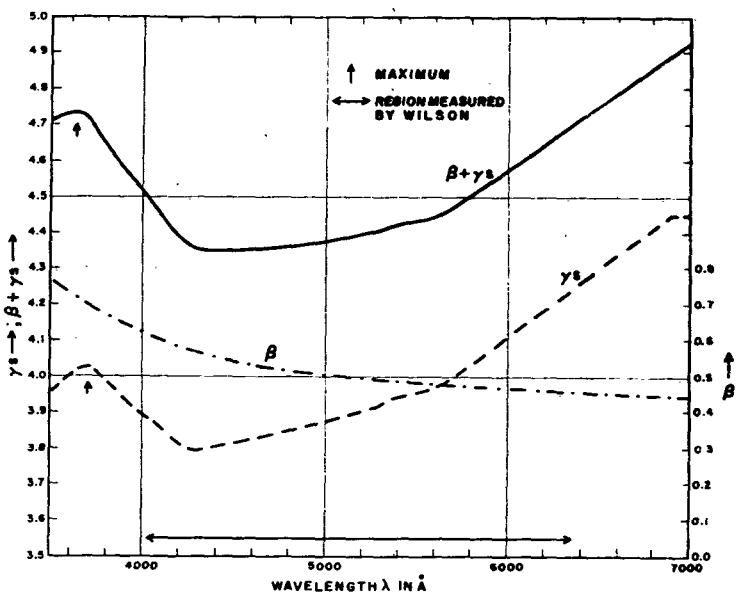

Fig. 9. The extinction coefficient β, γs and $\beta + \gamma s$ as a function of wavelength between 3500 Å and 7000 Å (blue sun). β is the extinction coefficient for normal clear atmosphere and air mass 1. γs is the extinction coefficient for the smoke layer, $\beta + \gamma s$ is the total extinction coefficient of the clear atmosphere plus the smoke layer on 26 and 27 September 1950.

(a) Case 1.
(b) Case 2.
(c) Case 3.

The regions measured by Wellmann and Wilson, respectively, are indicated by ←→.

Table 5. Extinction coefficients and absolute intensities of the solar radiation for the blue sun.
Steps 100 Å between 3500 Å to 7000 Å

Wave-length in Å	I_0 $\times 10^{-3}$ cal/cm² min 200 Å	β_λ	Case 1					Case 2				
			E	γ^s	I_A $\zeta = 53°$	I_A $\zeta = 61°$	I_A $\zeta = 67°$	E	γ^s	I_A $\zeta = 53°$	I_A $\zeta = 61°$	I_A $\zeta = 67°$
3500	23.7	0.755	2.32	1.026	1.23	0.59	0.24	2.73	1.554	0.514	0.205	0.064
3600	26.8	0.725	2.43	1.075	1.34	0.64	0.27	2.77	1.577	0.587	0.233	0.074
3700	30.5	0.695	2.60	1.151	1.43	0.67	0.27	2.81	1.600	0.674	0.268	0.085
3800	34.2	0.670	2.85	1.261	1.40	0.65	0.24	2.85	1.622	0.759	0.304	0.097
3900	40.0	0.644	3.04	1.345	1.48	0.68	0.24	2.92	1.663	0.868	0.345	0.109
4000	49.5	0.620	3.12	1.381	1.78	0.79	0.30	3.03	1.725	1.010	0.394	0.122
4100	55.0	0.595	3.215	1.423	1.93	0.88	0.31	3.11	1.771	1.083	0.419	0.129
4200	55.9	0.575	3.315	1.467	1.90	0.84	0.30	3.21	1.828	1.057	0.396	0.119
4300	57.0	0.562	3.50	1.549	1.71	0.74	0.26	3.29	1.873	0.998	0.378	0.112
4400	59.2	0.545	3.62	1.602	1.66	0.71	0.24	3.37	1.919	0.989	0.369	0.108
4500	61.0	0.530	3.71	1.642	1.65	0.67	0.23	3.45	1.964	0.970	0.358	0.102
4600	62.1	0.522	3.73	1.651	1.68	0.68	0.23	3.51	1.999	0.944	0.344	0.097
4700	62.9	0.515	3.80	1.682	1.63	0.69	0.23	3.58	2.038	0.906	0.327	0.091
4800	63.0	0.507	3.84	1.699	1.64	0.69	0.22	3.64	2.073	0.896	0.310	0.085
4900	62.5	0.500	3.92	1.735	1.50	0.63	0.21	3.70	2.107	0.825	0.290	0.079
5000	61.2	0.496	3.92	1.735	1.53	0.61	0.20	3.75	2.135	0.777	0.271	0.073
5100	59.7	0.492	3.90	1.726	1.49	0.60	0.20	3.79	2.158	0.734	0.254	0.068
5200	57.9	0.490	3.90	1.726	1.45	0.58	0.20	3.83	2.181	0.689	0.236	0.062
5300	57.3	0.488	3.90	1.726	1.43	0.57	0.19	3.87	2.204	0.653	0.223	0.058
5400	56.0	0.484	3.90	1.726	1.40	0.62	0.20	3.91	2.226	0.622	0.211	0.054
5500	55.5	0.481	3.90	1.726	1.39	0.61	0.19	3.93	2.238	0.610	0.205	0.053
5600	55.0	0.478	3.91	1.730	1.37	0.61	0.19	3.95	2.249	0.600	0.200	0.051
5700	54.6	0.473	3.94	1.743	1.37	0.60	0.19	3.97	2.261	0.584	0.195	0.050
5800	54.4	0.472	3.91	1.730	1.41	0.60	0.20	3.98	2.266	0.577	0.193	0.050
5900	54.3	0.470	3.84	1.699	1.47	0.60	0.21	3.99	2.272	0.576	0.191	0.048
6000	53.7	0.469	3.79	1.677	1.50	0.64	0.22	4.00	2.278	0.564	0.187	0.047
6100	52.8	0.466	3.75	1.659	1.53	0.69	0.23	4.01	2.283	0.549	0.183	0.046
6200	51.5	0.462	3.71	1.642	1.55	0.67	0.24	4.02	2.289	0.536	0.177	0.045
6300	50.3	0.460	3.68	1.628	1.56	0.70	0.24	4.02	2.289	0.523	0.174	0.044
6400	49.4	0.454	3.66	1.619	1.58	0.69	0.24	4.01	2.283	0.524	0.176	0.045
6500	48.4	0.451	3.64	1.610	1.60	0.67	0.25	4.00	2.278	0.522	0.175	0.045
6600	47.9	0.448	3.60	1.593	1.63	0.72	0.26	3.99	2.272	0.522	0.176	0.046
6700	47.1	0.445	3.58	1.584	1.60	0.70	0.26	3.98	2.266	0.523	0.177	0.046
6800	46.3	0.442	3.55	1.570	1.62	0.74	0.27	3.96	2.255	0.536	0.179	0.046
6900	45.8	0.440	3.48	1.540	1.69	0.78	0.29	3.94	2.243	0.531	0.182	0.048
7000	45.3	0.434	3.37	1.491	1.86	0.86	0.33	3.92	2.232	0.540	0.186	0.049

Table 5. Extinction coefficient and absolute intensities of the solar radiation for the blue sun — Concluded.

Wavelength in Å	Case 3					
	E	γ^s	I_A $\zeta = 53°$	I_A $\zeta = 61°$	I_A $\zeta = 67°$	I_A $\zeta = 71°$
3500	3.13	3.956	0.0095	1.45×10^{-3}	1.37×10^{-4}	1.23×10^{-5}
3600	3.17	4.007	0.0104	1.55	1.47	1.30
3700	3.19	4.032	0.0119	1.81	1.69	1.51
3800	3.16	3.994	0.0149	2.30	2.23	2.05
3900	3.12	3.994	0.0199	3.17	3.22	3.07
4000	3.08	3.893	0.0276	4.54	4.76	4.71
4100	3.06	3.867	0.0334	5.61	6.02	6.13
4200	3.02	3.817	0.0381	6.57	7.32	7.72
4300	3.00	3.792	0.0414	7.36	8.23	8.86
4400	3.01	3.805	0.0433	7.60	8.63	9.31
4500	3.02	3.817	0.0449	7.87	8.88	9.67
4600	3.03	3.830	0.0445	7.94	9.01	9.72
4700	3.04	3.843	0.0454	7.94	8.99	9.65
4800	3.05	3.855	0.0452	7.88	8.91	9.55
4900	3.06	3.867	0.0449	7.75	8.72	9.33
5000	3.07	3.880	0.0430	7.48	8.39	8.94
5100	3.08	3.893	0.0412	7.14	7.98	8.43
5200	3.09	3.906	0.0392	6.76	7.51	7.90
5300	3.10	3.918	0.0382	6.56	7.24	7.59
5400	3.12	3.944	0.0360	6.12	6.68	6.93
5500	3.13	3.956	0.0352	5.95	6.47	6.68
5600	3.14	3.969	0.0343	5.78	6.26	6.42
5700	3.16	3.994	0.0329	5.51	5.90	5.99
5800	3.19	4.032	0.0308	5.03	5.35	5.33
5900	3.22	4.070	0.0290	4.72	4.87	4.77
6000	3.25	4.108	0.0269	4.32	4.38	4.20
6100	3.28	4.146	0.0250	3.95	3.93	3.71
6200	3.31	4.184	0.0231	3.59	3.52	3.26
6300	3.34	4.222	0.0212	3.26	3.35	2.86
6400	3.37	4.260	0.0198	2.99	2.84	2.54
6500	3.40	4.298	0.0188	2.73	2.54	2.23
6600	3.43	4.336	0.0171	2.51	2.31	1.99
6700	3.46	4.373	0.0158	2.31	2.07	1.76
6800	3.49	4.411	0.0146	2.11	1.86	1.55
6900	3.52	4.449	0.0137	1.94	1.68	1.38
7000	3.56	4.500	0.0128	1.78	1.52	1.22

by atmospheric constituents. Other data of β were also used; however, since β contributes only a small amount to the total extinction, such differences are really insignificant. For unit air mass β decreases steadily from 0.755 at 3500 Å to 0.434 at 7000 Å, as shown in Fig. 9 and Table 5.

The extinction of the smoke particles is calculated in steps of 100 Å, using Eq. (1) and the thickness s = 3.7 km for cases 1, 2 and 3. The results obtained are reproduced in Fig. 9 and in Table 5.

The anomalous extinction is significantly different between cases 1 and 2 on one side and case 3 on the other. Over Hamburg it is small in the blue and red regions, and reaches a maximum at 4900 Å in case 1 and 6200 Å in case 2. The differences for γs in cases 1 and 2 arise from the different E functions used; case 2 is the more realistic one. Over Edinburgh a distinct minimum occurs at 4300 Å, the extinction being large in the ultraviolet and red parts of the spectrum. In all three cases, $\gamma s \gg \beta$: for 3500 Å it is greater by a factor of 1.5, 2 and 5 for cases 1, 2 and 3, respectively, and for 7000 Å by a factor of 3, 4 and 10 for cases 1, 2 and 3, respectively. Thus, the various values of β to choose from did not alter the result. Moreover, slight changes of the normal atmospheric transparency between the two days Wellmann and Wilson selected are without any significance to the result.

The narrow region measured by Wellmann is clearly conceived from the diagrams. The linearity of γs is more or less restricted to a small interval he measured. The total extinction $\beta + \gamma s$ is also plotted in Fig. 9 and the numerical results are given in Table 5. For Wellmann's observation, both cases show that the total extinction is small in the blue part of the spectrum and the maxima occur at 5700 Å. For Wilson's observation, the total extinction shows a broad minimum between 4200 Å and 5600 Å.

6. SPECTRUM OF COLORED SUN

6.1. SPECTRUM AND INTENSITY OF A "BLUE" SUN

The next step is to calculate the solar radiation on the ground using Eqs. (2) and (3). The values for $I_{0\lambda}$ are taken from Linke (1943); the extinction coefficients $\beta + \gamma s$ are taken from Table 5 as described in Section 5, and thus $I_{N\lambda\zeta}$ and $I_{A\lambda\zeta}$ are calculated in steps of 100 Å for the region 3500 Å to 7000 Å, and for the zenith distances ζ = 53°, 61°, 67° and 71°. The spectral region was selected for two reasons, first, the absorption due to ozone and water vapor can be neglected; second, the human eye is sensitive only in this region. The zenith distances selected correspond to Dietze's, Wellmann's and Wilson's observations.

The absolute values of the total radiation received on the ground are very small, only a fraction of what is received on a normal clear day. If the radiation incident on the atmosphere

$$I_0 = \int_{\lambda=3500\,\text{Å}}^{\lambda=7000\,\text{Å}} I_{0\lambda} d\lambda$$

and $I_{N\zeta}$ as well as $I_{A\zeta}$ are calculated accordingly, the ratio $I_{A\zeta}/I_0$ indicates very clearly the radiation received on the ground. The numerical results as found in Table 6, show that the solar radiation I_0 is reduced by a factor 10^{-3} to 10^{-6}. Furthermore, the variation caused by the zenith distances is extremely large (i.e., by a factor of 10 for going from 67° to 53°). Thus it is seen that the smoke layer reduces the solar radiation tremendously, comparable to a thin water cloud.

Table 6. Direct solar radiation received at the ground.
The ratio I_N/I_0 corresponds to a normal clear day, the ratio I_A/I_0 for the "blue sun" observations, and the ratio I_A'/I_0' for Dietze's observation. All ratios refer to the region 3500 Å to 7000 Å only, except those measured by Dietze.

Zenith distance	Computed				Observed
	I_N/I_0	I_A/I_0			I_A'/I_0'
		Case 1	Case 2	Case 3	
53°	0.43	0.03	0.014	5.6×10^{-4}	0.15
61°	0.35	0.013	0.0049	9.4×10^{-5}	....
67°	0.28	4.7×10^{-4}	1.4×10^{-4}	1.0×10^{-5}	....
71°	0.23	....	....	1.2×10^{-6}	....

Table 7. Ratio of relative intensities for the wavelength, where the intensity of the blue sun is a maximum.

Case	1		2		3	
λ_{max} in Å	4100		4100		4600 and 4700	
Zenith distance	I_A/I_0	I_A/I_N	I_A/I_0	I_A/I_N	I_A/I_0	I_A/I_N
53°	1.40	1.69	1.79	2.16	1.14	1.21
61°	1.46	1.86	2.06	2.63	1.18	1.26
67°	1.65	2.21	2.46	3.29	1.22	1.38
71°	....	....	....	....	1.30	1.48

Note: The abbreviated notation I_A/I_0 is used for: $\frac{I_{A,\lambda}}{I_{A,5500}} \Big/ \frac{I_{0,\lambda}}{I_{0,5500}}$ and similar for I_A/I_N.

Dietze observed a larger value of 15 percent for I_A'/I_0' on 28 September. The reason for this discrepancy of our values and the observed one is threefold. First, the reduction was largest on 27 September and, therefore, N_T must have been smaller when he took his observations; second, the actinometer measured the red and infrared radiation too, which is excluded from our calculations. The contribution from the red part of the spectrum is large. Furthermore, his red ratio (Table 1) indicates this fact, which is due to the decrease of E with wavelength (part (a) of Fig. 1). Third, the actinometer has a large angular aperture of several degrees, and sky radiation around the sun is measured also. As Dietze's data show (Table 1), the sky radiation is much larger than normal ($H/I = 2.4$ instead of 0.09 on a clear day). If I_A/I_0 was about 0.1 in Dietze's case, N_T may be assumed to be 3.5×10^7 (1/cm² column). Such a variation seems very reasonable and the total amount certainly varied (see Section 6.3).

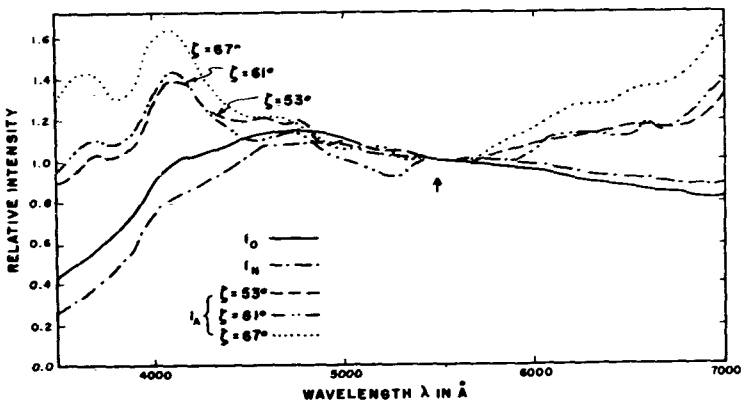

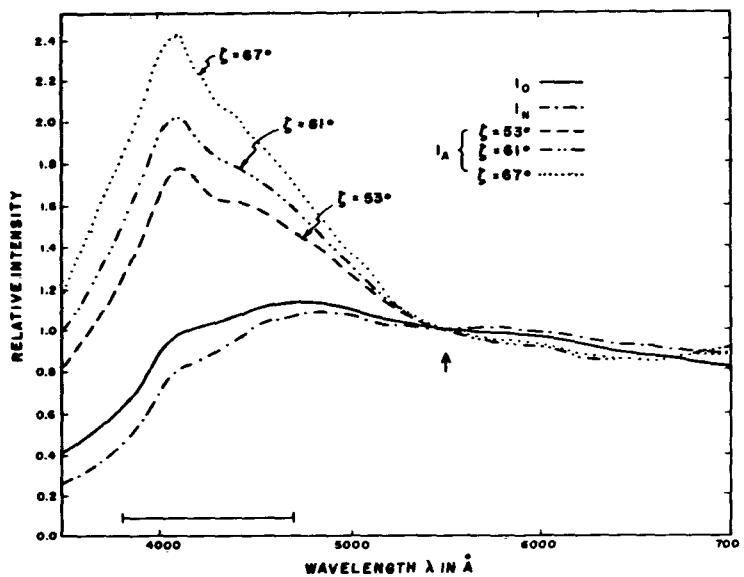

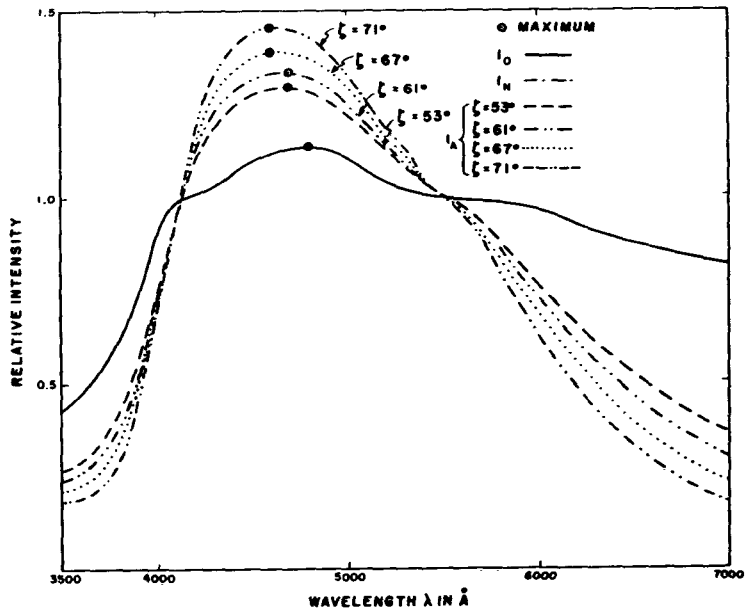

Fig. 10. Spectral intensity distribution of the solar radiation between 3500 Å and 7000 Å, in relative units.

I_0 **intensity outside the atmosphere.**

I_N **intensity on the ground on a normal clear day for zenith distance of the sun** $\xi = 53°$.

I_A **intensity on the ground on a day with the "blue sun" for zenith distance of the sun** $\xi = 53°, 61°, 67°$ **and** $71°$.

The relative intensity 1.0 is chosen for $\lambda = 5500$ Å, **the peak of eye sensitivity.**

(a) **Case 1.**
(b) **Case 2.**
(c) **Case 3.**

The most interesting features of the spectrum are obtained from Fig. 10. Here relative values are plotted using $I_0 = I_A = I_N = 1.0$ for $\lambda = 5500$ Å, corresponding to the maximum sensitivity of the eye. The most impressive spectrum is certainly that of Fig. 10 (b) for case 2, but the outstanding characteristic, the maximum in the blue, is the same in all three cases. The intensity in the blue increases with increasing zenith distance, if relative values as defined above for Fig. 10 are used. For $\lambda = 4100$ Å, the relative intensity is 1.8 times $I_{0\lambda}$ for $\zeta = 53°$, and 2.4 for $\zeta = 67°$ for case 2 and smaller for case 3 as seen from Table 7.

The increase in the yellow and red parts of the spectrum starts in case 1 which is already at 5700 Å, and in case 2 at 6700 Å. Thus case 2 is certainly more realistic from this point of view also. This increase is a consequence of the E function, which decreases rapidly from the first maximum towards 0 for $\alpha = 0$ or $\lambda \to \infty$ as can be seen from Fig. 1, as well as from Figs. 5 and 6. Case 3, Fig. 10 (c), shows a different behavior because the maximum in the blue stands out much clearer, even if this increase is smaller, as in cases 1 and 2 (Table 7). However, the relative intensity in the red part of the spectrum is much lower than the ratio $I_{0,\lambda}/I_{0,5500}$; at 7000 Å $I_{A,\lambda}/I_{A,5500}$ is less than one-half of $I_{0,\lambda}/I_{0,5500}$, where as in case 2 it is nearly equal.

The results of the calculations definitely confirm that the energy distribution of the solar spectrum has been completely altered and that a maximum exists in the blue region, provided that the radius of the particles is about 0.4 to 0.6 μ and that the total number is very large, namely, $\approx 10^8$/cm. These are the two important conditions which cause a "blue" sun.

In the various general descriptions of the "blue" sun of September 1950, reports are also given of the same phenomenon after dust storms near desert regions. In such cases the particles are probably quartz dust. The refractive index of quartz is $m = 1.55$. This value is not much larger than the values used in this calculation, and from Table 4 it can be concluded that the particles must be smaller, about 0.3 to 0.5 μ and the number $\gg 10^8$/cm^2 column. If these conditions are fulfilled, then the solar spectrum is similar to that of Fig. 10 and the sun may look blue in color.

6.2. HYPOTHETICAL SPECTRUM OF A "GREEN" SUN

A green sun or moon has been reported very rarely in the literature. One British observer, however, states that on 26 September 1950 the moon was rising as a normal orange-yellow, but later the color was something between a sea-green and a turquoise-blue.

It can be concluded from Fig. 2 that the radius of the particles must be close to 1 μ for a minimum of extinction in the green. Thus a calculation similar to that of the blue sun described above was carried out, using $r_0 = 0.963$ μ, $N_T = 2 \times 10^7$/cm^2 and three size distributions. Case 4, $r = r_0$, uniform size; case 5, same size spectrum as in case 2, with $h = 7.07$; case 6, size spectrum with $h \approx 10$, i.e., a much narrower distribution. The zenith distances chosen are 53°, 61°, 67° and 75°. The results of the calculations are given in Fig. 11 for two zenith distances. The general trend can be obtained from the selected results as published in Table 8.

A relatively sharp maximum can be obtained only for a very narrow distribution of particles. The reason for this is that the broader the size spectrum, the less pronounced is the minimum in the E function (see Fig. 1). There is practically no minimum if $h < 7$ or $\sigma > 0.1$, which means that the anomalous extinction is more or less independent of wavelength. Such a neutral extinction shows no color effects. The intensity maximum becomes more pronounced with increasing zenith distance. Hence, only for a sun and moon close to the horizon can the green color effect be observed. With the sun or moon high above the

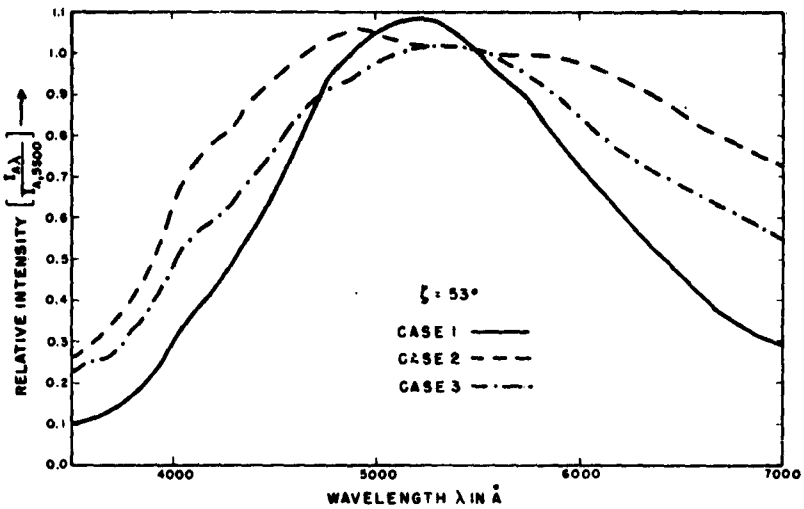

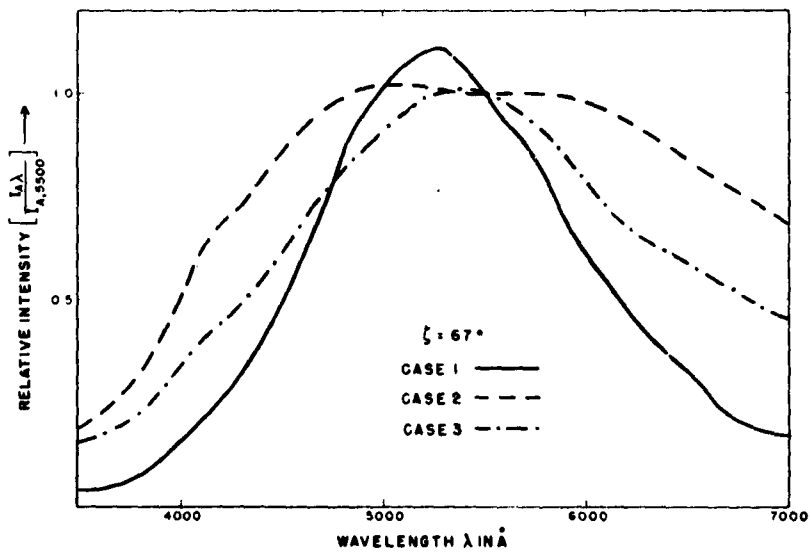

Fig. 11. Spectral intensity distribution of the solar radiation between 3500 Å and 7000 Å, in relative units for a "green sun."
(a) Refers to cases 1, 2 and 3 and zenith distance of the sun $\zeta = 53°$.
(b) Refers to cases 1, 2 and 3 and zenith distance of the sun $\zeta = 67°$.
The relative intensity 1.0 is chosen for $\lambda = 5500$ Å.

horizon, the color must return to the normal color of the objects. The conditions for a green sun are very severe:

(1) $r \approx 0.9$ to 1.0 μ and a *very* narrow size spectrum.

(2) $N_T \gg 10^7/\text{cm}^2$ column.

Table 8. Relative intensities $I_{A\lambda\zeta}/I_{A\zeta 5600}$ for a green sun.
Three wavelengths are selected, namely, 3500 Å, 7000 Å and λ_{max}.
Constants chosen are: $r_0 = 0.963\ \mu$, $N_T = 2 \times 10^7/\text{cm}^2$ column, $\zeta = 53°, 61°, 67°$ and $75°$.

Case 4: uniform size

λ in Å	ζ 53°	61°	67°	75°
3500	0.11	0.075	0.049	0.016
5300	1.08	1.10	1.11	1.15
7000	0.30	0.23	0.17	0.079

Case 5: size spectrum, $h = 7.07$

λ in Å	ζ 53°	61°	67°	75°
3500	0.26	0.22	0.20	0.13
4900	1.05	1.02	....	....
5100	....	....	1.02	....
5300	....	....	....	1.00
7000	0.73	0.70	0.69	0.62

Case 6: size spectrum, $h = 10$

λ in Å	ζ 53°	61°	67°	75°
3500	0.23	0.19	0.15	0.09
5400	1.01	1.01	1.02	1.02
7000	0.56	0.51	0.46	0.34

For quartz: $m = 1.55$, the same results are obtained as calculated above, if:

(1) $r \approx 0.58\ \mu$

(2) $N_T \geqq 5.6 \times 10^7/\text{cm}^2$ column.

6.3. PHYSIOLOGICAL IMPRESSION OF SUCH SPECTRA

What subjective impression does such a spectral distribution of solar light as received by the eye produce in the brain of the human observer? This is a physiological and no longer a physical problem. We shall deal only with an observer whose color sensitivity is normal.

The mechanism of color vision is but partially understood at the present time. The most important problem with regard to atmospheric optics is the interpretation of spectrophotometric data by the eye. The theory developed by Helmholtz is based upon the fact that any color stimulus can be matched visually by a mixture of the proper amounts of three arbitrarily chosen stimuli, which are called primaries.

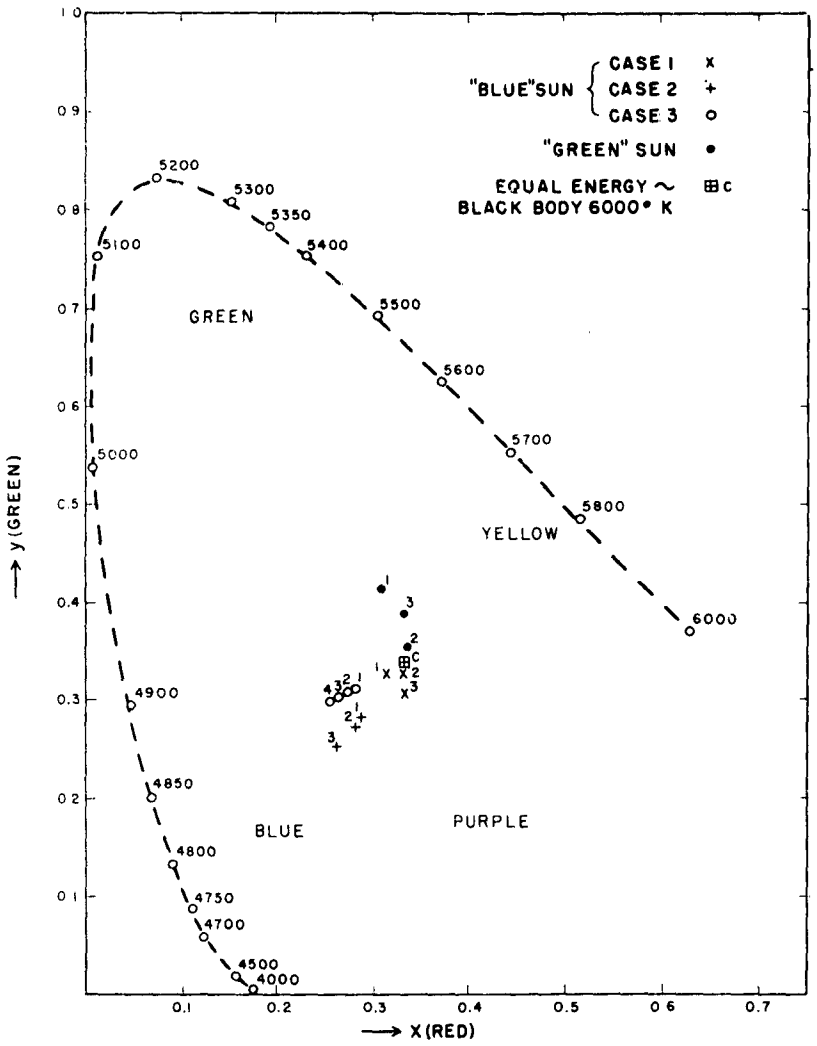

Fig. 12. Chromacity diagram for a green and a blue sun. A description of this diagram is given in the text. The numbers refer to zenith distances of the sun.

The excitation functions of the eye for three such primaries are defined by the International Commission on Illumination for an equal-energy spectrum. But the relative magnitudes of the three functions have been chosen so that the areas under the curves are equal for mean noon sunlight. The graphical representation of color is best carried out in a color triangle using the three excitation functions, or in an ordinary Cartesian coordinate system, as shown in Fig. 12. If the values are normalized, with x_1 = red, y_1 = green and z_1 = blue, according to

$$x = \frac{x_1}{x_1 + y_1 + z_1}; \qquad y = \frac{y_1}{x_1 + y_1 + z_1}; \qquad z = \frac{z_1}{x_1 + y_1 + z_1}$$

it suffices to plot x and y, because only two of the three quantities are independent. Each point in this diagram represents a certain color.

On this diagram point C represents the center of gravity and corresponds to the solar spectrum as seen on the earth. Furthermore, it shows the locus of spectrum stimuli as a series of circles starting in the lower left corner. These are the points for pure monochromatic colors between 4000 Å and 6000 Å. A straight line from C to any of the spectrum loci includes all points representing the stimuli obtained by additive

Table 9. Trichromatic coefficients x, y and z, dominant wavelength (λ_d) and colorimetric purity (p) for the blue and green solar spectra as functions of zenith distance ζ and particle size spectrum.

(a) *Blue Sun*

Case 1

ζ	53°	61°	67°
x (red)	0.327	0.330	0.333
y (green)	0.314	0.314	0.309
z (blue)	0.339	0.356	0.356
λ_d	4850	....	....
p	0.07	negative	negative
color	blue	purple	purple

Case 2

ζ	53°	61°	67°
x (red)	0.286	0.278	0.261
y (green)	0.283	0.273	0.262
z (blue)	0.430	0.449	0.477
λ_d	4750	4700	4750
p	0.21	0.24	0.32
color	blue	blue	blue

Case 3

ζ	53°	61°	67°	71°
x (red)	0.282	0.274	0.265	0.257
y (green)	0.313	0.309	0.305	0.299
z (blue)	0.405	0.417	0.429	0.444
λ_d	4850	4850	4850	4850
p	0.18	0.22	0.25	0.28
color	blue	blue	blue	blue

(b) *Green Sun* zenith distance = 67°

	Case 4	Case 5	Case 6
x (red)	0.308	0.336	0.333
y (green)	0.415	0.355	0.389
z (blue)	0.277	0.309	0.278
λ_d	5350	5600	5550
p	0.17	0.05	0.16
color	green	yellowish-green	yellowish-green

mixture in various portions of the extremes of the spectrum. Therefore, it is called a mixture (or chromacity) diagram.

There are other factors besides chromacity which determine the color, e.g., hue, saturation and brilliance. Three objective parameters are chosen to correspond in a general way with these physiological attributes. They are:

(1) dominant wavelength
(2) colorimetric purity
(3) brightness (or luminosity).

The dominant wavelength is defined as the wavelength where a straight line between C and the color point intersects the curve for pure monochromatic radiation (spectrum locus). The colorimetric purity is the ratio of the luminosity of the monochromatic radiation to the total luminosity. The luminosity is simply the sum of the luminosities of the monochromatic radiation and white radiation.

These considerations are now applied to the spectra calculated in Sections 6.1 and 6.2. The numerical constants and formula are taken from Judd (1933) and the results are condensed in Table 9 and plotted on Fig. 12. In the case of the "blue" sun, case 1 gives values for the uniform particle size which are very close to the solar color (crosses in Fig. 12). The purity is 0.07 for $\zeta = 53°$; for the other two the color should be white with a purplish hue. Thus this poor result shows that Wellmann's data cannot be interpreted by particles of uniform size. But in case 2 the values are better; the dominant wavelength is about 4750 Å, which is blue. The colorimetric purity is 0.2 to 0.3. Finally, the results for case 3 resemble those for case 2; the dominant wavelength corresponds to a blue color and the colorimetric purity is 0.18 to 0.28. The colorimetric purity increases with increasing zenith distance. The color should not be pure blue, but a rather bluish white, because the colorimetric purity is 0.2 to 0.3 for the zenith distances in question. From these data it is seen that the sun or moon is blue near the horizon and becomes more and more the normal yellow - white the higher it is in the sky. It is also seen that the color effect only occurs for particles having a size spectrum and not for those of uniform size.

For the green sun, the results of the calculations are summarized in Table 9 (b) and in the mixture diagram. The values for zenith instances $\zeta = 67°$ show that an effect only occurs for very uniform particles; the colorimetric purity is 0.17 for uniform particles, for a relatively small spread of $h \approx 10$ it is 0.16, but for a wide distribution with $h = 7$ it is only 0.05. The color of the pure spectrum locus is green in all three cases. The colorimetric purity also increases with increasing zenith distance, as for the blue sun.

The final computations show very clearly that the physiological impression of the spectra calculated in Section 6.1 is a bluish-white. Furthermore, the chromacity diagram proves that Wellmann's and Wilson's physical measurements confirm the numerous observations of a blue sun during September 1950. It has been argued by Elvey (1934) that the appearance of a blue sun, during the observations of a duststorm in 1934 was a "psychological" and not a "physiological" effect, and was dependent on the change of contrast between sun and sky. Since he used only a blue and yellow filter and not spectroscopic measurements — as did Wellmann and Wilson — his conclusions are based on insufficient physical data. This study endeavors to show distinctly that very precise spectroscopic observations are required to deduce such data as given in Sections 4, 5 and 6.

These studies confirm that the observers were correct in describing a "blue" sun. This phenomenon was not fictitious, but real. It occurs very rarely, simply because the conditions for its occurrence are very severe; namely, the radius must be around 0.5 μ, the size distribution must be narrow and the total number larger than $10^8/cm^2$ column.

7. REFERENCES

Aden, A. D. and M. Kerker (1951), "Scattering of Electromagnetic Waves From Two Concentric Spheres," *J. Appl. Phys.* 22, 1242.

Bull, G. A. (1951), "Blue Sun and Moon," *Meteor. Mag.* 80, 1.

Dietze, G. (1951), "Die Anomale Truebung der Atmosphaere September/Oktober 1950," *Zeits. Meteor.* 5, 86.

Elsley, E. M. (1951), "Alberta Forest Fire Smoke — 24 September 1950," *Weather* 6, 22.

Elvey, C. T. (1934), "Some Observations of the Sun Through a Dust Storm," *Monthly Weather Rev.* 62, 201.

Foitzik, L. (1950), "Zur Meteorologischen Optik von Dunst und Nebel, *Zeits. Meteor.* 4, 289, 321.

Gebke, W. (1951), "Bemerkungen zum Phaenomen der blauen Sonne," *Zeits. Meteor.* 5, 82.

Holl, G. (1946, 1948), "Lichtstreuung an dielektrischen Kugeln vom Brechungsexponent $n = 4/3$," *Optik* 1, 213 and 4, 173.

Houghton, H. G. and W. R. Chalker (1949), "The Scattering Cross Section of Water Drops in Air for Visible Light," *J. Opt. Soc. Amer.* 39, 955.

Hulst, H. C. van de (1949), "The Solid Particles in Interstellar Space," *Rech. Astron. de l'Obs. d'Utrecht* XI, part 2.

Judd, D. B. (1933), "The 1931 I.C.I. Standard Observer and Coordinate System for Colorimetry," *J. Opt. Soc. Amer.* 23, 359.

Linke, F. (1942), "Handbuch der Geophysik," 8, Borntraeger, Berlin.

Linke, F. (1943), "Meteorologisches Taschenbuch," 4, 238, Akadem. Verl., Leipzig.

Pepperhoff, W. (1951), "Ueber die Dispersion des optischen Absorptionsvermoegens von Flammenrussen," *Optik* 8, 354.

Rodewald, M. (1952), "Die blaue Sonne vom 27 September 1952," *Naturw. Rundsch.* 5, 8.

Wellmann, P. (1951), "Die Blaufaerbung der Sonne am 27 September 1950," *Zeits. Astrophys.* 28, 310.

Wexler, H. (1950), "The Great Smoke Pall — 24–30 September 1950," *Weatherwise* 3, 129–134.

Wilson, R. (1951), "The Blue Sun of September 1950," *Mon. Not. Roy. Astr. Soc.* 111, 478.